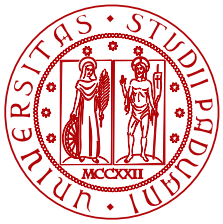

UNIVERSITÀ
DEGLI STUDI
DI PADOVA

Dipartimento
di Fisica
e Astronomia
Galileo Galilei

ASTRONOMY AND PHYSICS DEPARTMENT

MASTER'S DEGREE IN ASTROPHYSICS AND COSMOLOGY

Smoldering Embers: The Search for Slowly-cooling White Dwarfs in Globular Clusters NGC 288 and NGC 362

Supervisor
Prof. Antonino P. Milone

Candidate
Sofia Lionetto

ACADEMIC YEAR 2023-2024

Graduation date 19/06/2024

To my family and to Alyssa,
the guide stars of my life.

Abstract

Recent observational evidence suggests the existence of a new class of White Dwarfs in the populations of several Globular Clusters, deviating from the standard cooling sequence due to what is thought to be residual hydrogen burning in their envelopes. The presence of such WDs seems correlated with the Horizontal Branch morphology of their host cluster, as they have so far only been detected in clusters with HBs featuring an extended blue tail. This work examines two galactic globular clusters known for their distinct HB morphologies, NGC 288 and NGC 362, using data collected from Hubble WFC3-UVIS in the F275W and F336W ultraviolet bands. Starting from the raw images, I used state-of-the art programs to reduce the images and derive the cluster color-magnitude diagrams through single-pass and multi-pass photometry. Said diagrams are then used to re-derive cluster ages, metallicities, distance moduli and reddening coefficients by means of by isochrone fitting. The obtained values are then checked against the literature, and a morphological comparison of the two cluster CMDs is performed. Finally, using the information thus gained, the white dwarf cooling sequences of both clusters are analyzed, with a focus on their luminosity functions. The luminosity function of NGC 288 WDs significantly deviates from theoretical expectations for standard cooling, as found in M13 and NGC 6752, while no such anomaly is detected in the WD luminosity function of NGC 362, in line with what observed in M3 and M5. In the conclusions I then explore a number of possible explanations for the observed differences in the WD sequence between the two cluster types.

Riassunto

Recenti analisi osservative suggeriscono l'esistenza, in alcuni ammassi globulari, di una nuova tipologia di Nane Bianche, il cui processo di raffreddamento presenta anomalie dovute, secondo recenti modelli teorici, ad un residuo bruciamento dell'idrogeno nei loro starti esterni. La presenza di queste NB sembra essere correlata alla morfologia del Ramo Orizzontale dell'ammasso di appartenenza, essendo state finora rilevate solo in presenza di una sequenza molto estesa nel blu. Questo lavoro esamina due ammassi globulari della Via Lattea noti per avere rami orizzontali molto diversi tra loro: NGC 288 e NGC 362, usando dati raccolti dalla WFC3-UVIS del telescopio spaziale Hubble nei filtri ultravioletti F275W e F336W. Partendo dai file immagine grezzi, riduco le immagini tramite programmi allo stato dell'arte e ottengo i diagrammi Colore-Magnitudine dei due cluster tramite fotometria single- e multi-pass. I diagrammi vengono quindi usati per riderivare età, metallicità, moduli di distanza e coefficienti di reddening dei due ammassi tramite fit di isocrone. I valori ottenuti vengono quindi confrontati con la letteratura, e si procede a un confronto morfologico tra i diagrammi dei due ammassi. Infine, con le informazioni ottenute, si procede all'analisi delle rispettive sequenze di raffreddamento delle NB, con particolare attenzione rivolta alle loro funzioni di luminosità. Si constata come la funzione di luminosità di NGC 288 differisca in modo sostanziale dalle previsioni teoriche per un normale raffreddamento, al pari di M13 e NGC 6752, mentre lo stesso fenomeno non si presenti in NGC 362, in linea con quanto osservato in M3 e M5. Infine nelle conclusioni esploro alcune possibili spiegazioni per le differenze osservate tra le sequenze NB dei due tipi di ammassi.

Contents

Chapter 1

Introduction

According to modern astrophysical literature, most stars in the Universe are thought to complete their life-cycle as White Dwarfs (WDs). These stellar remnants are mostly composed of electron-degenerate matter from the former star's core - its outer layers ejected during the final stages of its evolution - surrounded by a thin envelope of hydrogen and helium. With gravitational collapse halted by the Pauli exclusion principle and lingering nuclear reactions being generally considered negligible, WDs have no substantial means to increase or maintain their internal energy. Their evolution, therefore, has been characterized as a cooling process, one that modern theoretical models aim to predict in detail. In fact, our theoretical understanding of white dwarf cooling has been used to obtain information about the ages of stellar populations both simple and complex, such as star clusters, the Milky Way halo, or its disk (see [1] and references therein).

However, recent analyses of the white dwarf cooling sequences of a select number of clusters by Chen *et al.* (2021-2023) [2]–[4], as well as previous study from Torres *et al.* (2015) [5] have detected a number of high-temperature, high-luminosity WDs in excess of theoretical expectations, considered possible evidence for the existence of a class of slower-cooling white dwarfs. Intriguingly, this anomaly does not present itself in all clusters examined, but only in those among them who exhibit a Horizontal Branch (HB) with an evident and extended blue tail [6].

As HB morphology depends on cluster metallicity, this would seem to support recent theoretical models predicting the possibility, for very metal poor stars, to skip the Asymptotic Giant Branch (AGB) phase and evolve directly into hydrogen-rich white dwarfs. These dwarfs would be capable of sustaining significant nuclear reactions in their envelopes, slowing their cooling [7]–[9].

It must be noted, however, that cluster metallicity isn't the only factor at play. In particular, the M3-M13 cluster pair examined in [2] is a well-known "second parameter couple", presenting very different horizontal branch morphologies despite similar metallicity. Of the two, only M13, with its extended blue HB, presents evidence for an excess of bright white dwarfs. This could potentially

imply a connection between the anomalous cooling of these dwarfs and the still uncertain "second parameter" behind the differences in cluster HB morphology.

However, the number of clusters examined so far is still too low to draw any definite conclusions. The aim of this work is therefore to carry out an independent analysis of two additional metal-poor globular clusters: the second parameter pair of NGC 362 and NGC 288, to check whether a similar phenomenon is observed and to compare and contrast the results obtained with those available in the literature.

This thesis will be structured as follows:

Chapter 1 will give a brief introduction to globular clusters, stellar populations, white-dwarfs and their cooling sequences.

Chapter 2 will detail the targets of this study, their physical characteristics as found in the literature, and the data used in this study.

Chapter 3 will examine, step by step, the data reduction process used to obtain accurate photometric catalogues from the initial images.

Chapter 4 will cover data analysis, from the preliminary isochrone fitting to the comparison between the WDCSs of each cluster.

Chapter 5 finally, will explore a number of possible causes for the results present the conclusions of this work.

1.1 White Dwarfs

The class of stellar remnants known as white dwarfs, first discovered in the 1910s [10] makes up about 7% of nearby stars [11]. Current astrophysical knowledge estimates, in fact, that all stars with initial mass between 0.07 and 8-10 $M_{\odot}$ (over 95% of the total) will end their stellar evolution as such an object [1]. Their mass is on the order of $M_{\odot}$, while their radius is comparable with that of the Earth, making them far denser than ordinary matter. Their effective surface temperatures span an extremely wide range: from over 150000K to near 4000K, with the most common observed values ranging from 16000 K to 8000 K. Due to their high effective temperatures and very small radii they are visible as white-blue, faint objects, placing them in the bottom left of the Hertzsprung-Russel (or Color-Magnitude) diagram, away from the main sequence [12].

According to current astrophysical knowledge, white dwarfs are composed of a mixed carbon-oxygen core[1], the electrons of which are in a degenerate state, their pressure opposing the gravity-induced collapse. This structure explains the extremely high density of these stellar remnants and places a strong limit on their maximum mass: the Chandrasekar mass limit at $\sim 1.4\ M_{\odot}$. The core is surrounded by a thin shell mostly composed of helium $\sim 10^{-2} M_{\odot}$, which can in turn be surrounded by an even thinner hydrogen envelope, accounting for $\sim 10^{-4} M_{\odot}$ [1].

The theoretical range of possible WD masses is therefore very limited compared to their progenitors, and, observationally, sharply peaked around $0.6\ M_{\odot}$. This is regarded as evidence of the important role played by mass loss in stellar evolution, and of the largely self-regulating nature of the mechanisms leading to outer shell expulsion in its final stages. That said, more massive progenitor stars do correspond to (slightly) more massive WDs, even if, somewhat unintuitively, a larger mass will correspond to a smaller radius, due to the different equilibrium point between gravitational forces and electron pressure. [12]

Having exhausted or expelled the vast majority of their hydrogen and helium, white dwarfs are generally thought to have no significant lingering nuclear reactions contributing to their internal energy. Additionally, the degenerate pressure of the electrons in their core strongly hinders any kind of collapse, keeping the radius mostly static and preventing significant internal energy to be gained from gravitational potential variations. Therefore, for most of their evolution, white dwarfs have no means to increase their internal energy [2] [16], which can only be gradually radiated away[3]. In this sense, white dwarf evolution can be described as a cooling process. As this process is predicted to last around 10^{10} years, no fully cooled "Black Dwarfs" are expected to exist in the Universe at the current epoch.

1.1.1 White Dwarfs as Cosmic Clocks

Due to their clearly stratified, relatively simplistic structure, apparent cooling-like evolution, and much reduced dependence on factors critical in active stars (such as the specifics of nuclear reactions, metal content and convective mixing [1], [17]), the potential of using white dwarfs as "cosmic clocks" to date stellar populations has been recognized as early as the 1950s (see Schimdt 1959) [18]: given knowledge of the relation between WD luminosity and age, a stellar population could be dated by observing its dimmest white dwarfs.

[1] White dwarfs of especially low or high mass could potentially possess helium, or mixed oxygen, neon and magnesium cores respectively. [13], [14]

[2] An important exception is the case of core crystallization, which is predicted to happen at very late stages of white dwarf evolution, at $t \sim 10^9$ and was recently confirmed by Gaia observations - see e.g. Tremblay *et al.* (2019) [15]

[3] Mostly through emission of photons, as neutrino emission is predicted to only be relevant for the first few Myrs of WD evolution [1]

A first estimate of white dwarf cooling was calculated by Leon Mestel in 1952 [16]:

$$t_{cool}^{Mestel} \propto A^{-1}\mu^{-2/7}M^{5/7}L^{-5/7} \tag{1.1}$$

However, as showed by Van Horn in 1971 [19], this cooling law is based on several simplifying assumptions and approximations, none of which hold valid beyond the first, high temperature stages of WD evolution, and more reliable estimates require more detailed (and complex) numerical calculations. Until the turn of the century, the refinement of these models was slowed down not only by computational requirements, but also by the intrinsic faintness of these objects, which strongly limited our ability to observe all but the brightest of them in a relatively small volume around the Earth. Now, however, with the introduction of 8m- and 10m-class ground telescopes, and the proliferation of space telescopes of increasing sensitivity, accuracy and resolution (e.g. Hubble, Gaia, Swift) we have almost complete samples of disk WDs in a large volume around us, and it is possible to study the brightest WDs of even halo globular clusters. Theoretical predictions can then be compared with accurate observations, and their approximations and theoretical assumptions adjusted to better match the available data, in an iterative improvement process which is still ongoing to this day (see [9], [12], [20] and references therein for a detailed history of this progress).

1.1.2 Slow Cooling White Dwarfs

The assumption of pure cooling is however merely a very good approximation: theoretical calculations show that, due to very high core temperatures[4] and high pressure due to strong surface gravity, conditions at the bottom of the WD gas envelope can sustain residual nuclear burning, contributing to the dwarf's internal energy. These reactions, while marginal, persist until the very late stages of WD evolution, as derived by Iben & MacDonald (1985, 1986) [21], [22]. Their intensity depends on the mass of the white dwarf's hydrogen envelope, which in turn is influenced by the metal content of its stellar progenitor. In the case of a solar metallicity progenitor this effect is only predicted to be relevant for a few million years, but in the case of stellar progenitors with very poor metallicity ($Z \sim 0.001$ or less) and consequently thicker WD hydrogen envelopes, calculations show that residual nuclear burning can be significant for up to $\sim 10^9$ years - see e.g. Renedo *et al.*, (2010) [9]. Due to its apparently marginal influence on cooling rates, this effect has not been considered until recently, when cooling tracks for white dwarfs with metallicity well below this value have been computed. Bertolami et al. (2013) [23] showed that, for progenitor metallicities comparable to $Z \lesssim 10^{-4}$, and low mass ($M_{WD} \lesssim 0.6M_{\odot}$, $M_{ZAMS} \lesssim 1M_{\odot}$), the

[4] On the order of $10^7 K$ in the initial states of WD evolution [12]

residual hydrogen burning can release enough energy to significantly delay cooling for an extended time period. This can lead to much longer cooling times at high to intermediate luminosities than in the case of solar metallicity progenitors [8], [21], [22]. It must be noted that these conditions, while stringent and not common in the disk, are satisfied by a significant portion of stars in the galactic halo and in the oldest globular clusters. They should therefore have an identifiable impact on observations of those targets.

1.2 Globular Clusters

Globular clusters are gravitationally bound, compact spheroidal aggregates of tens of thousands to millions of stars. They appear to be present in all galaxies and, in the case of the Milky Way (and other spirals), appear concentrated in the galactic halo and bulge. More than a century of study of their stellar populations, starting with the work of H. Shapley and A. Sandage [24], [25], has revealed that they are old (generally ~ 10 Gyr, with mounting evidence of a possible role in galaxy assembly or even cosmic reionization) and that the stars in each cluster are not only spatially close, but also *approximately* coeval and chemically homogeneous [26].

Due to their status as evolved "simple stellar populations" (valid only in first approximation), the systematic observation of globular clusters - through astrometry, photometry and spectroscopy - has played a critical role in the development of stellar evolution theory, from the development of the first concepts of stellar physics such as the mass-luminosity relation at the beginning of the past century, to more and more advanced models, which have in turn been used to investigate cluster characteristics and, through them, the history of galactic star formation (see e.g. [27] and references therein).

The overall picture has been further complicated in recent years by the discovery that most GCs are actually host to *multiple* stellar populations. Thanks to new hardware (such as the ACS and WFC3 cameras for the Hubble Space Telescope) and software for precision photometry (such as that developed by Anderson *et al.* [28]), it is increasingly evident that their Color-Magnitude Diagrams (CMDs) are the sum of multiple sequences belonging to different "groups" or "generations" with slightly different chemical composition. The origin and nature of these populations, the reasons why they are present in some clusters and not others, and what they imply for their formation and evolution, is at the heart of modern research on globular clusters [29].

1.2.1 Horizontal Branch and Second Parameter Problem

The stars making up the horizontal branch of a cluster's CMD are stars of mass between 0.5 and $2.3\ M_{\odot}$ which are burning helium in their cores and hydrogen in a shell surrounding it. They tend to have very similar luminosities in the V-band (hence the name), due to very similar core masses. Their effective surface temperatures, on the other hand, can span a wide range, depending on the properties of their hydrogen envelopes[5].

It was found early on that the morphology of the horizontal branch depended on metallicity: metal rich clusters would present a redder branch, while metal poor ones a more extended, bluer one [30]. This is thought to be due to the effect of metallicity on the temperature of the hydrogen envelope surrounding the burning helium core [31], [32].

However, observations in the following years challenged this simplistic interpretation: some clusters with very similar metallicity would present drastically different HB morphologies, hinting at the presence of at least one additional parameter to explain this difference. Solving this "second parameter problem" has proved to be a challenge: more than half a century of intensive research has brought up a number of possible factors, such as cluster age, cluster density, or helium abundance, but no definite consensus has been reached so far [33]–[36].

With the recent discovery of multiple populations in globular clusters, it is also reasonable to assume that their horizontal branches may themselves be composed by sub-branches belonging to different groups/generations, and indeed recent findings suggest that multiple populations may play a role in HB morphology [37]–[39].

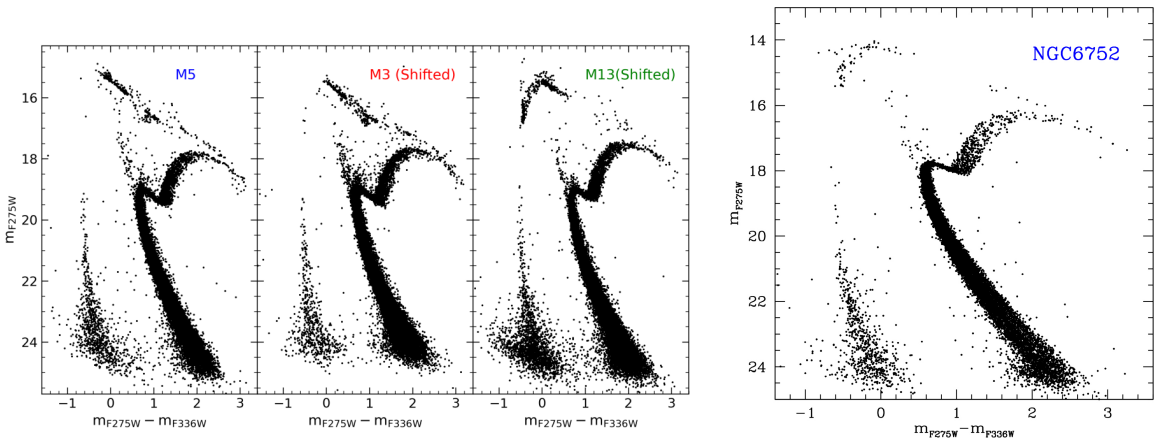

Figure 1.1: Color-magnitude diagrams of several second-parameter clusters (M3, M5, M15 and NGC 6752) from Chen *et al.* (2022-2023). It can be seen that while these clusters share similar metallicity values the morphology of their horizontal branch is quite different.

[5]Hence the Horizontal Branch not being horizontal when observed with different filters.

1.2.2 White-Dwarf Cooling Sequence (WDCS)

In a simple stellar population, such as that of an ideal cluster, differences in evolution are essentially driven by differences in the starting mass of each star. Massive stars evolve more rapidly while the opposite is true for low mass ones. The white dwarfs present at a given epoch therefore do not all have the same age, but rather a spread of ages depending on the cluster's initial mass function. Older white dwarfs are cooler and fainter than newer ones, which means that, on a CMD, cluster WDs will be spread out in a sequence extending from relatively high magnitudes for new ones to progressively lower magnitudes for older ones. It then stands to reason that a cluster of finite age would have a WDCS of finite extension, and that the age of the cluster itself might be derived by measuring said extension.

The purported independence of these sequences from the metallicity of their respective populations, and its reliance on different physics has provided astronomers with an alternative cluster dating method to the traditional main sequence turn-off determination, with which to cross check the available data.

Due to the faint luminosity of white dwarfs and the crowded nature of globular clusters, however, this dating method is limited by stringent resolution and photometric depth requirements, quickly growing prohibitive with increasing distance. It took until 2006 for the end of the white dwarf cooling sequence to be first detected in a globular cluster, thanks to the Hubble Space Telescope [40]. This started an ongoing effort to identify the end of the WDCS in several other clusters (see, e.g. [41]–[43]), though, due to the aforementioned observational hurdles, only some of the closest to Earth have been dated in this way. These observations have nonetheless proved instrumental in refining and validating theoretical models of WD cooling to the point where accurate WDCS luminosity function models for cluster of different ages are now available - see Salaris et al. (2008, 2013) [20], [44].

Despite the uncertainties involved (mostly centered about core composition and the approximations inevitably adopted in the models employed), these predictions have proved reliable when tested against available data, making the large discrepancies noted by Chen *et al.* - especially when limited to a single cluster of a second-parameter pair, as in [2] - all the more striking. For this reason, we will now examine exactly one such "second parameter couple": globular clusters NGC 288 and NGC 362.

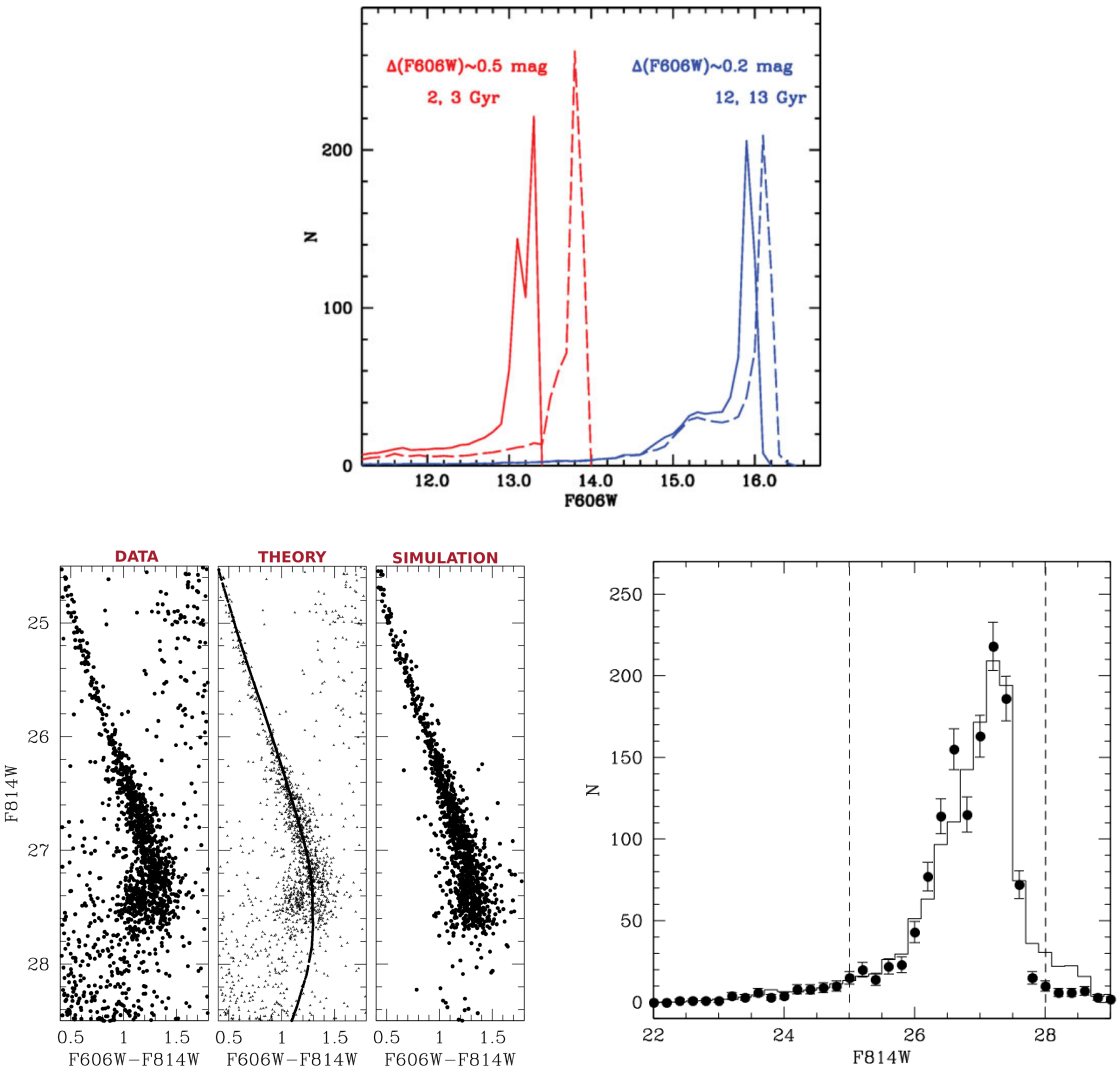

Figure 1.2: Two examples of the power of current theoretical models of white dwarf cooling - *Top:* Luminosity function models in the Hubble F606W filter for different cluster ages by Salaris *et al.* (2008). *Bottom Left:* A comparison between the observed WDCS of NGC 6397, the theoretical prediction of the cooling sequence for the cluster, and a simulation of said sequence created from the theoretical model with Monte-Carlo methods by Hansen *et al.* (2007). *Bottom Right:* the observed (dots) versus theoretical (histogram) WD luminosity function of the same cluster.

Chapter 2

Targets and Data

2.1 NGC 288 and NGC 362

The targets of this study are NGC 362 and NGC 288, two globular clusters in the galactic halo. According to the literature, both are relatively old (10-13 Gyr), have similar distance from the galactic center, similar mass range, similarly low metallicity ($[Fe/H] < -1$), and similar α-enhancement [45]. The morphology of their respective horizontal branches, however, is very distinct: the HB stars of NGC 362 lie almost exclusively on the red side of the RR-Lyrae instability strip, similarly to the case of M3, while the opposite is true for NGC 288 [46], whose horizontal branch has a stronger resemblance to that of M13. They are, in essence, a classic example of a second parameter cluster pair.

For this reason, both clusters have been the subject of extensive research aimed at identifying such parameter(s). The most studied one has been a possible age difference between the two clusters [47]–[50], though there have been studies suggesting that this difference may be very slight or negligible [51]. Other possible factors are central density (low for NGC 288, while NGC 362 might have undergone core collapse) [52], [53] and binary star fraction (significantly higher for NGC 288 than for NGC 362 [54]). Additionally, on the subject of multiple stellar populations, NGC 288 has been classified as a 'conventional', or Type I cluster, while NGC 362 has been classified as an 'anomalous', or Type II cluster, exhibiting a more complex population structure than the norm, with a wider range of chemical variations. This is in contrast with M3 and M13, which are both Type I clusters of similar age and central density, and whose binary fraction appears to be flipped, with M3 presenting more binaries than M13 [54]–[57].

While the relevance of each of these factors in shaping the HB of a cluster is not clear, the differences from the M13-M3 case will be of interest when comparing the results of this work with those from Chen *et al.*

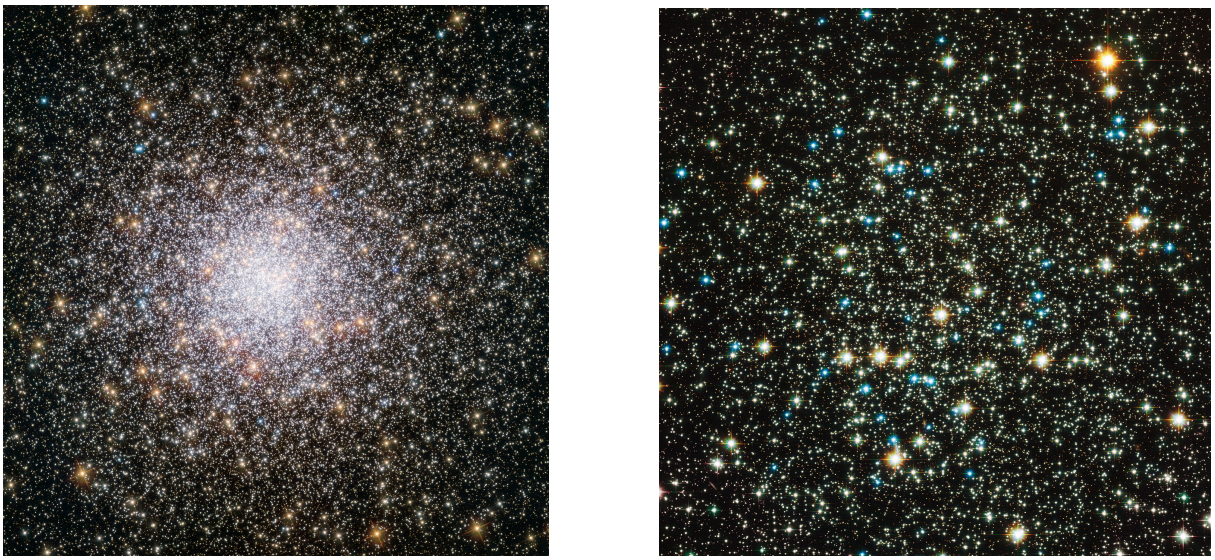

Figure 2.1: NGC 362 (*left*) and NGC 288 (*right*), the targets of this comparative study. (Image credit: NASA-HST)

2.2 Images

As previously mentioned, the observation of globular cluster white dwarfs is a highly demanding task due to both their low luminosity and distance. Moreover, the density of globular cluster cores, on the order of thousands of stars per square arcminute even for 'loose' clusters like NGC 288, requires very high spatial resolutions. This favors space observatories such as the Hubble Space Telescope (HST), as they do not suffer the effects of atmospheric seeing.

At the same time, the clusters' locations, at almost $\sim$10Kpc from the galactic center, suggest a very low reddening coefficient for both, which is confirmed both by data from NASA's Galactic Dust Reddening and Extinction Service[1], and from previous studies of the same clusters [60][61]. Given this, and the high surface temperature of young white dwarfs, the wavelength range best suited to this study is in the UV range, closer to the emission peak of these objects[2].

Given the wavelength, photometric sensitivity, and resolution requirements, the most suitable data for our analysis is that collected by HST during two observing runs carried out between 2012 (PI: Piotto, see [60]) and 2016 (PI: Kalirai, see [62]). These images map the central region of the two clusters in the F275W and F336W ultraviolet filters, using the UVIS sensor of Hubble's Wide Field Camera 3 (WFC3) [63].

[1] Based on the work of Schlegel, Finkbeiner and Davis (1998)[58], and Schlafly and Finkbeiner (2011)[59] on CORBE, IRAS and SDSS data respectively. More info can be found at:
`https://irsa.ipac.caltech.edu/applications/DUST/`

[2] For reference, the Planckian emission peak for a 1Gyr old white dwarf with an expected surface temperature on the order of 10^5K is around 300nm

In particular, this work will make use of the `flc` files, which are science frames already corrected for factors such as spatial noise, bias, eventual dark currents, etc. and for image defects related to charge-transfer efficiency (CTE) [64]. A set of `drc` files, corrected for geometric distortion and all of the above factors, and normalized to an exposure time of 1s, will be used for calibration.[3]. These images will have to be properly reduced in order to derive the photometric catalogs needed for our analysis. A detailed breakdown of the files used in this work can be found in Tab. 2.2

[3]For more info, see: `https://hst-docs.stsci.edu/wfc3dhb/chapter-2-wfc3-data-structure/2-1-types-of-wfc3-files`

Name	Filter	Exp.(s)	Date	Program	Cluster	PI
icyf01jnq	F275W	650	18/09/16	14155	NGC 362	Kalirai
icyf01k4q	F275W	650	18/09/16	14155	NGC 362	Kalirai
icyf01k6q	F275W	700	18/09/16	14155	NGC 362	Kalirai
icyf01kaq	F275W	700	18/09/16	14155	NGC 362	Kalirai
icyf01keq	F275W	680	18/09/16	14155	NGC 362	Kalirai
ibpd07d6q	F275W	519	14/09/12	12605	NGC 362	Piotto
ibpd07daq	F275W	519	14/09/12	12605	NGC 362	Piotto
ibpd07dcq	F275W	519	14/09/12	12605	NGC 362	Piotto
ibpd08jrq	F275W	519	09/09/12	12605	NGC 362	Piotto
ibpd08jvq	F275W	519	09/09/12	12605	NGC 362	Piotto
ibpd09jxq	F275W	519	09/09/12	12605	NGC 362	Piotto
ibpd07d8q	F336W	350	14/09/12	12605	NGC 362	Piotto
ibpd07deq	F336W	350	14/09/12	12605	NGC 362	Piotto
ibpd08jtq	F336W	350	09/09/12	12605	NGC 362	Piotto
ibpd08jzq	F336W	350	09/09/12	12605	NGC 362	Piotto
ibpd05uqq	F275W	400	25/10/12	12605	NGC 288	Piotto
ibpd05uuq	F275W	400	25/10/12	12605	NGC 288	Piotto
ibpd05uwq	F275W	401	25/10/12	12605	NGC 288	Piotto
ibpd06q2q	F275W	401	07/11/12	12605	NGC 288	Piotto
ibpd06qdq	F275W	400	07/11/12	12605	NGC 288	Piotto
ibpd06qfq	F275W	400	07/11/12	12605	NGC 288	Piotto
ibpd05usq	F336W	350	25/10/12	12605	NGC 288	Piotto
ibpd05uyq	F336W	350	25/10/12	12605	NGC 288	Piotto
ibpd06q4q	F336W	350	07/11/12	12605	NGC 288	Piotto
ibpd06qhq	F336W	350	07/11/12	12605	NGC 288	Piotto
ibpd0720	F275W	1557	14/09/12	12605	NGC 362	Piotto
ibpd0730	F336W	700	14/09/12	12605	NGC 362	Piotto
ibpd0520	F275W	1201	25/10/12	12605	NGC 288	Piotto
ibpd0530	F336W	700	25/10/12	12605	NGC 288	Piotto

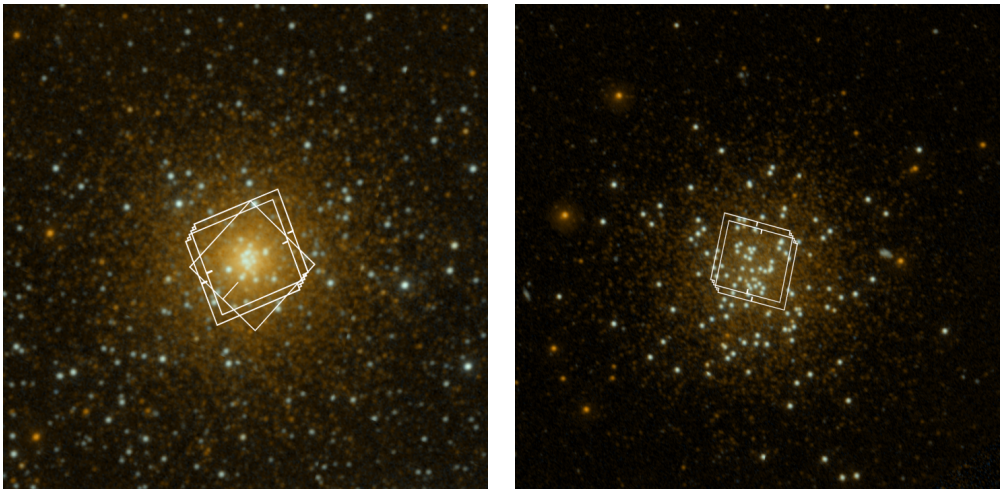

Figure 2.2 & Table 2.1: *Table:* All the image files used in this work. The first 25 are `flc` files. The last 4 are the `drc` files that have been used for calibration. *Bottom images:* combined footprint of said exposures for NGC 362 (left) and NGC 288 (right) (Image Credit: NASA-GALEX)

Chapter 3

Data Reduction

Once the appropriate `flc` *.fits files corrected for bias, spatial noise and CTE have been selected and obtained, they must be properly reduced to extract the relevant photometric information.

The reduction pipeline will be modeled after that used in the globular cluster surveys by Nardiello *et al.* [65] and Milone *et al.* (2023) [66] (both of which make heavy use of WFC3-UVIS data), both in the criteria employed and in the photometry software used. Data will be handled by means of custom Python code making use of the `numpy` and `pandas` libraries [67], [68].

3.1 Single-Pass Photometry

As a preliminary step, I perform first-pass photometry on each individual file with the software suite developed by Jay Anderson for HST images [28], specifically a version modified for use with WFC3-UVIS [69]. Rather than performing aperture photometry, this program selects stars and measures their flux by empirically calculating their Point Spread Function (PSF). The program starts by dividing an image in a `nxn` grid, and performs a preliminary fit on the bright, isolated, unsaturated stars of each section using manually provided PSF libraries [1]. Then, in an iterative process, the residuals from the previous fit are used to improve the PSF model itself. To account for spatial variations, the expected PSF model for the remaining stars is then calculated by interpolating the four closest grid PSFs according to the relative distance of each star from the brighter ones [70]. As the PSF can change slightly between exposures due to factors such as focus variations or residual CTE, the procedure is repeated separately for each image.

The PSFs thus obtained are then used to measure position and magnitude of each unsaturated object in the image, while saturated ones are measured according to the procedure detailed in

[1] http://www.stsci.edu/~jayander/STDPSFs/

[71], [72]: a preliminary aperture photometry measurement in a 5 pixel radius is supplemented with the contribution from contiguous saturated pixels outside that radius. This information is then recorded in a preliminary catalogue for each image.

To remove spurious datapoints from our catalogues we filter them based on the value of their quality-of-fit parameter, or qfit. This value, calculated in a 5x5 pixel grid around each detected object, is a measure of how well the empirical PSF fits the object, and is defined by the equation:

$$qfit = \frac{\sum_{x,y} pixel_{x,y} PSF_{x,y}}{\sqrt{\sum_{x,y} pixel_{x,y}^2 PSF_{x,y}^2}} \tag{3.1}$$

where $pixel_{x,y}$ and $PSF_{x,y}$ are respectively the actual recorded value and that of the best-fitting PSF model for the x, y pixel. The qfit is, in effect, simply a way to express the linear correlation coefficient between the former and the latter. While it is expected that fainter objects will tend to deviate from the expected PSF due to a lower signal-to-noise ratio, it is reasonable to assume that any outliers with qfit significantly smaller than the average for a given magnitude might be non-stellar objects or artifacts.

I therefore divide the catalogue in half-magnitude intervals, compute the median and standard deviation of the qfit value for each, and reject all outliers with qfit value significantly below the median. I set the rejection threshold at 5σ.

The root mean square deviation associated with the magnitude measurement is also recorded for each object. While it would ordinarily be a good estimator of measurement quality, we opt not to use it in the selection process at this stage: given that the dataset includes observations taken at different epochs, a magnitude error cut-off could potentially exclude variable stars presenting magnitude variations between exposures.

3.1.1 Catalogue matching

The filtered catalogues obtained from each image are then merged into two master catalogues (one per each cluster) with the following procedure: a photometric master frame is chosen for each bandpass (from the images with the deepest exposure). With software assistance, stars from each image catalogue are matched with those of the master frame by means of a six-parameter linear transformation. For increased accuracy, the matching is performed in two steps: a preliminary estimate of the parameters is first derived for bright, unsaturated stars, then used as a base for an improved calculation. Geometric distortion due to camera, sensor and filter characteristics is accounted for with the methods and solutions developed by Bellini *et al.* [73], [74].

The instrumental magnitudes associated with the stars in each frame are also brought to the zero-point of the master frame by calculating the mean of the magnitude difference between bright, unsaturated stars in the master frame and their match in each exposure. As a final step, the master catalogues for each filter are appropriately matched with each other, and the coordinate system brought into alignment with that based on the Gaia Early Data Release 3 [75], with the x coordinate matching the West direction and the y coordinate matching the North direction.

3.1.2 Calibration

The final catalogue thus obtained is then calibrated to the Vega magnitude system. For each filter, I use aperture photometry (with a 0.4 arcsec radius) to calculate the magnitudes of bright and unsaturated stars in the respective `drc` image files (cfr Tab. 2.2), which are drizzled, corrected for CTE and normalized to an exposure time of 1s. Then, by matching the resulting catalogue with the one derived from the `flc` files, I calculate, for each filter, the median (clipped to 3σ to exclude outliers) of the difference between the instrumental magnitude values derived from PSF photometry and those derived from aperture photometry on the drc files. Finally, the resulting medians, combined with the aperture corrections and zero-point values of the corresponding filters [76], [77], are added to all stars in the PSF photometry catalogue to obtain the calibrated magnitudes.

3.1.3 First-pass CMDs

After this data reduction process the Color-Magnitude diagrams for both clusters are finally available (See Fig. 3.1). The most apparent difference between the two clusters lies, as expected, in the morphology of their horizontal branches: in NGC 288 the near totality of detected HB stars are concentrated on the bluer end, away from the Red Giant Branch, appearing extremely bright in UV due to their high surface temperature. Meanwhile the horizontal branch of NGC 362 presents a slightly more even distribution, but one strongly concentrated towards the fainter, redder end, near the cluster RGB.

Other visible differences include a more distinct binary Main Sequence (MS) in NGC 288 (due to it having a higher proportion of binaries [54], [78]) and different subdivisions in the red-giant branches of each cluster - which are due to differences in the stellar population makeup of each cluster, whose chemical variations the employed filters are highly sensitive to [79]–[81]. Otherwise, the two cluster CMDs appear remarkably similar, due to their comparable age and very similar metallicity.

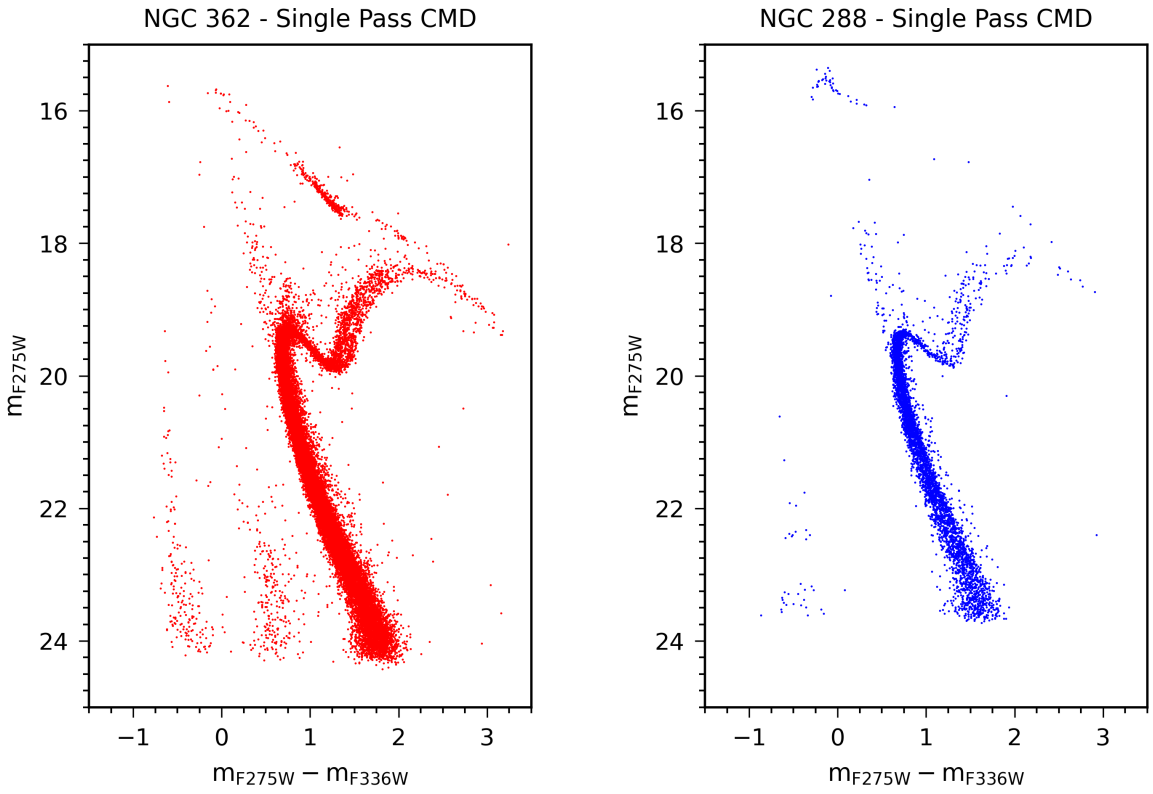

Figure 3.1: Color-Magnitude Diagrams for NGC 362 (red, left) and NGC 288 (blue, right) obtained through single-pass photometry. Note the morphological differences between the respective Horizontal Branches. In the case of NGC 362 CMD, the extra sequence between MS and WDCS is due to the presence of SMC stars in the background.

Proper motions and the Magellanic Cloud

The stars forming the extra central sequence in the NGC 362 CMD are not part of the cluster, but rather main sequence stars belonging to the Small Magellanic Cloud, which is very close in terms of celestial coordinates even if much further away ($\sim 200 Kpc$). This can be demonstrated by a rudimentary check of their proper motions: as cluster exposures were taken in different epochs, and bulk motions for cluster stars and SMC stars are different [53], it is reasonable to expect the coordinate matching transformation used to create the master photometric catalogue to have been less accurate for SMC stars, resulting in a larger coordinate error [28].

Indeed, when the catalogue is filtered according to the total positional error, most the datapoints eliminated belong to the central sequence, with minimal variations elsewhere. The well-defined location of these stars on the CMD suggests that the background contamination for the cluster WDCS is very low and will not have significant effects on the following analysis, though a follow-up study including a full proper motion analysis for better filtering is desiderable.

3.2 Multi-Pass Photometry

To improve the magnitude range and statistics of the cluster CMDs - and their respective WDCSs in particular, I use the first-pass photometry data as input for the multi-pass photometry FORTRAN software KS2[2], developed by J. Anderson ([65], [82], [83]).

The program identifies and measures stellar positions and magnitudes simultaneously across all images by means of an iterative procedure: in each iteration, KS2 identifies the most bright and best-isolated stars in each image, proceeds to calculate their magnitudes, positions, errors and shape parameters, then subtracts them from the image and repeats the process on the remaining stars. With each pass, progressively fainter and less isolated stars will be identified and measured, down to the noise floor. The simultaneous nature of the measurement across multiple images makes it possible to find and measure stars that are not detectable in all frames.

To aid in the identification and measurement of faint stars particularly close to bright ones, the data from first-pass PSF photometry is used to generate masks for the brightest stars (both saturated and not).

In the interest of maximum accuracy, the photometry itself is carried out in three different modes, each detailed in [83]:

- The first mode is optimized for bright stars: the program searches for peaks within 5x5 pixel squares and, upon finding one, uses the best-fitting local PSFs derived during first-pass photometry to measure stellar magnitudes and positions after subtracting neighboring stars. The relative sky background is computed from an annulus between 4 and 8 pixels from each star.

- The second mode, optimized for stars too faint to allow for an optimal PSF fit: all neighboring stars are subtracted, then aperture photometry is performed in a 5x5 pixel area centered on the target. Each pixel is appropriately weighted in order to minimize contamination by nearby sources. The sky background, meanwhile, is computed as in the first method.

- The third mode, a modification of the second optimized for crowded environments: the steps are the same as above, but the photometry radius is limited to 0.75 pixels from the central peak, while the sky background annulus is smaller: from 2 to 4 pixels from the star's centroid.

It's important to note that none of the methods employed measure saturated stars - the single-pass photometry catalogues remain the best source for that information.

[2] Informally, 'Kitchen Sink 2'

All three methods are used, and the results compared. Careful inspection confirms that method two is the most effective with regards to faint stars, such as those on the cluster WDCS. Therefore, I decide to use the results obtained with this method for my analysis.

For the removal of spurious and unreliable datapoints from the multi-pass photometry catalogue I employ the same qfit filtering employed in the single-pass case: I compute the median value and the standard deviation of the qfit for every half-magnitude interval, calculate the corresponding 5σ threshold, interpolate between the values so obtained, and reject all datapoints with a qfit value beyond this threshold.

I also add another selection criterion: a shape parameter called RADXS, calculated in an annulus between 1 and 2.5 pixels from the center of the object and defined by [84]:

$$RADXS = \frac{\sum_{x,y} pixel_{x,y} - PSF_{x,y}}{10^{-mag/2.5}} \tag{3.2}$$

This parameter, which is normalized to the object's flux, measures the difference between the detected flux and that predicted by the PSF model used. It is easy to see that it is positive when the object is wider than expected (e.g. in the case of extended objects like background galaxies) and negative when the object is sharper than expected (e.g. point-like artifacts due to cosmic rays). The ideal situation, when the flux exactly matches that of the fitted PSF, corresponds to $RADXS = 0$, but it can be expected, much like in the case of qfit, that this value will progressively deviate from that with increasing magnitude.

I therefore employ a similar outlier rejection method, determining the median value of the shape parameter for each half-magnitude interval, calculating the $\pm 5\sigma$ thresholds, linearly interpolating between the values so obtained and rejecting all datapoints with a RADXS beyond the resulting lines.

The root mean square error of the magnitude data is also considered. I find that, while most of the datapoints follow the expected trend (with RMS increasing with magnitude), a significant fraction of objects at every magnitude has a RMS value of *exactly* 9.999 (see Fig. 3.2). I take this to be indicative of a measurement error, and exclude these points from the analysis.

This selection is performed separately for each filter, then combined so that only datapoints satisfying all criteria in both filters are kept. Fig. 3.3 shows the rejected datapoints for cluster NGC 362.

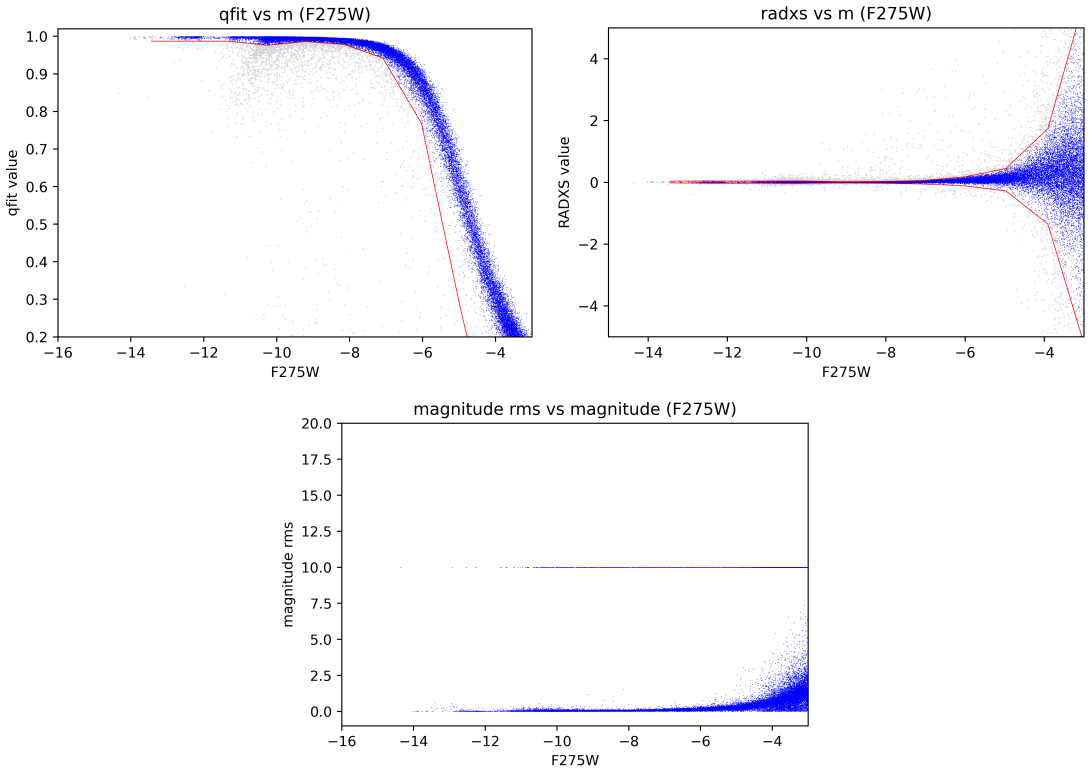

Figure 3.2: Selection criteria for NGC 362 multi-pass data in the FW filter. In order: qfit (upper left), RADXS (upper right), and magnitude RMS error (bottom). The red line marks the interpolated 5σ rejection threshold. Rejected datapoints are indicated in gray.

3.2.1 Multi-pass CMDs

After applying the same calibration procedure used in the case of first-pass photometry, we once again obtain the two CMDs (Fig. 3.4). As can be readily seen, optimizing the multi-pass parameters for dim objects has had the expected trade off: a loss of detail at brighter magnitudes, with e.g. the split RGBs and the binary MS in NGC 288 being no longer easily identifiable, compensated by both CMDs now reaching two full magnitudes lower (down to F275W $\sim$ 26). The magnitude floor, where flux peaks of stellar origin are of the same order as the noise, is visibly slanted due to the fact that, for bluer objects, the F336W filter data is the primary source of noise due to lower signal, but the depth and overall statistics of both WDCSs - the actual targets of this study - are much improved from the single-pass case.

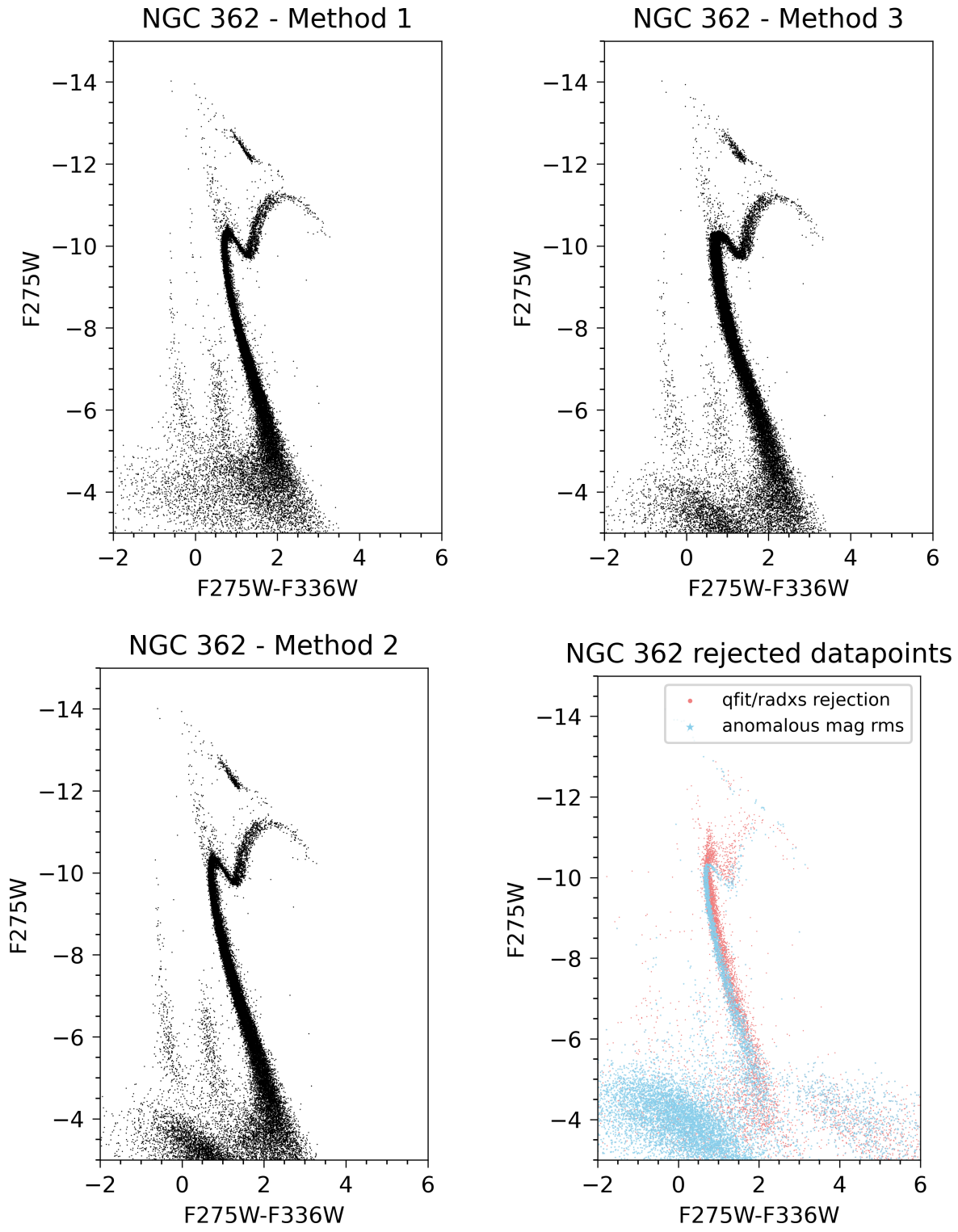

Figure 3.3: Color-(Instrumental)Magnitude Diagrams for NGC 362 obtained through the three possible multi-pass photometry methods, after applying the selection criteria described in Sec.3.2. Compare and contrast WDCS statistics and noise for each. On the bottom right, the datapoints rejected from the method 2 dataset.

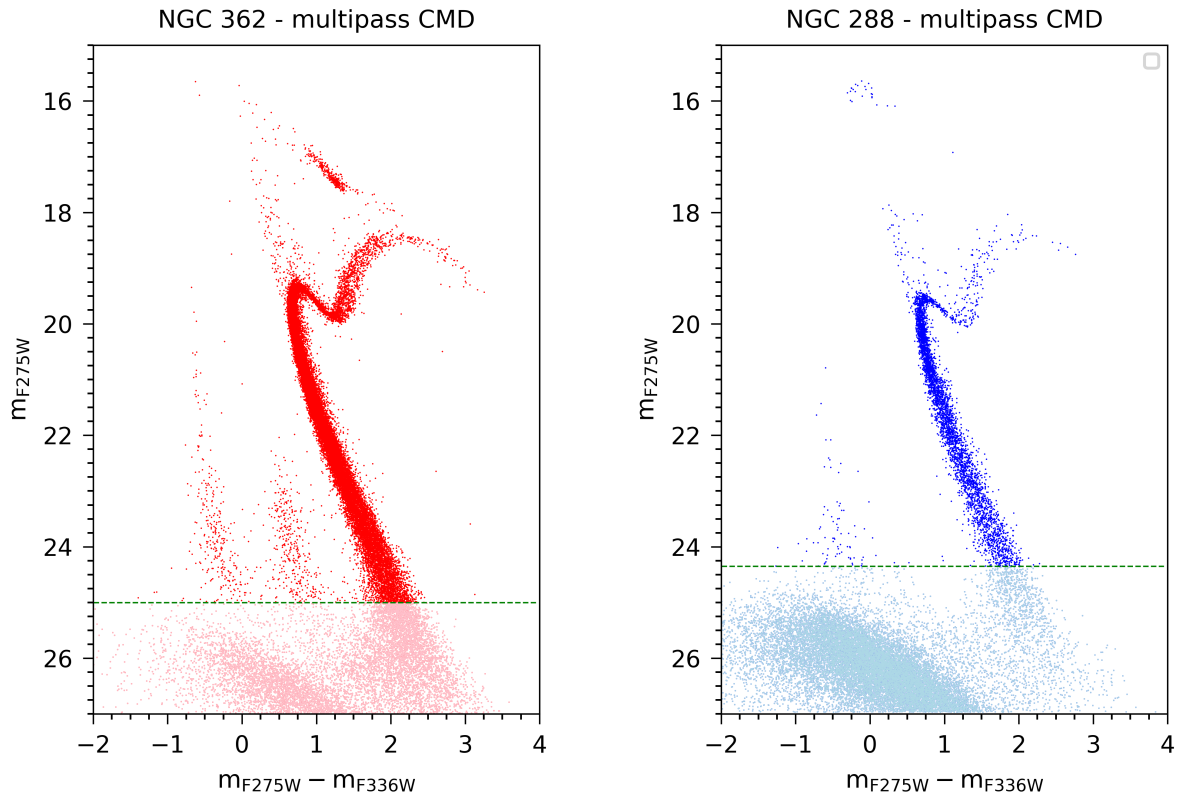

Figure 3.4: Color-Magnitude Diagrams for NGC 362 (red, left) and NGC 288 (blue, right) obtained through multi-pass photometry. The green dashed lines represent a conservative estimate of the noise floor for each cluster. Compare and contrast with Fig. 3.1

Chapter 4

Data Analysis

4.1 Isochrone Fitting

Before studying the WDCS proper, I aim to independently rederive a number of cluster characteristics (such as age, metallicity and distance modulus) through isochrone fitting. To that end, I opt to use the BaSTI stellar tracks and isochrone database, as it offers isochrone models for alpha-enhanced stellar populations [17], [85]–[87].

To find the best isochrone fit for each cluster, I adopt a multi-step procedure. Initially, a starting isochrone set is chosen based on the range of reddening, distance modulus and metallicity values reported in the literature. This initial set is then narrowed down by means of visual comparison with the obtained CMDs, focusing in particular on the relationship between age, metallicity, alpha-element enrichment, and the slopes of the main sequence and the RGB. This estimate is further refined by means of progressive and systematic variation of isochrone parameters, where at each step the quality of the isochrone fit is gauged by comparing the χ^2 value relative to the distance between an appropriate fiducial sequence placed on the CMD and each linearly interpolated isochrone.

The best isochrone fit for each cluster - that is, the one which minimizes the χ^2 value - can be seen in Fig. 4.1, while the relative parameters can be found in Tab. 4.1. As can be seen, the results are in good agreement with the literature, especially with regards to *relative* quantities such as metallicity and age differences between the two clusters [48], [88]–[91].

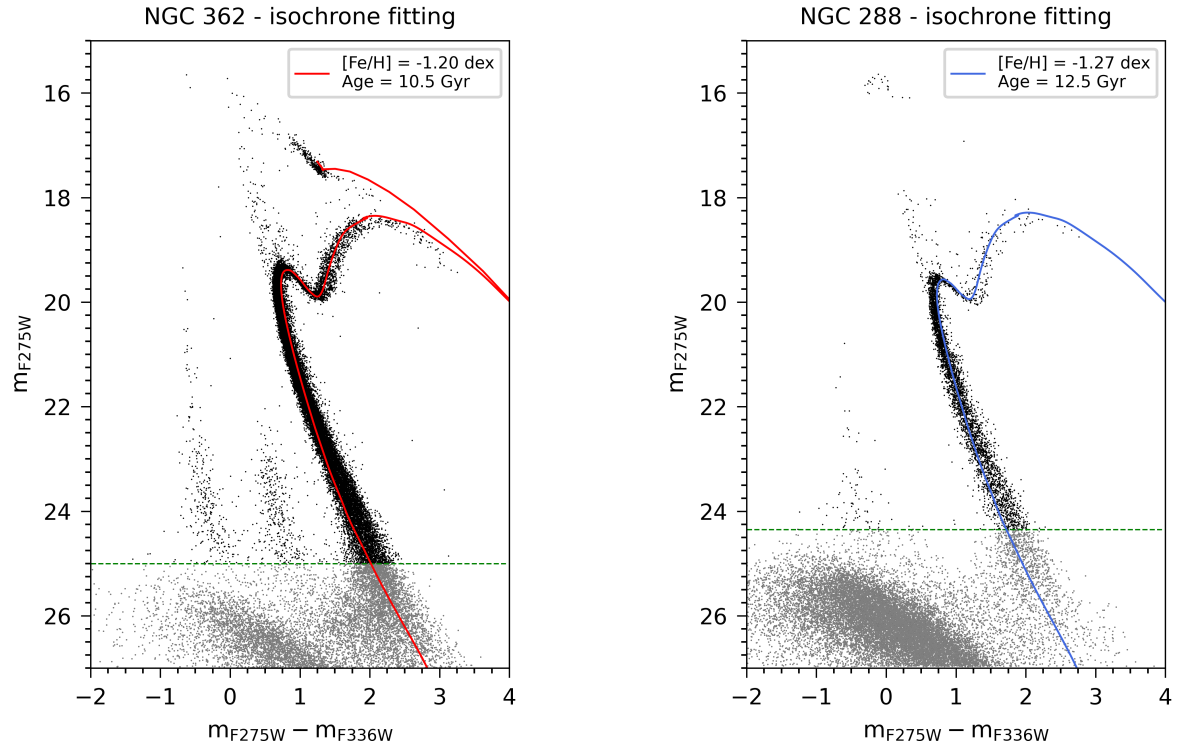

Figure 4.1: BaSTI Isochrone fitting of NGC 362 (in red) and NGC 288 (in blue). the fitting parameters used are reported in Tab.4.1

Cluster	Age (Gyr)	[Fe/H] (dex)	[α/Fe] (dex)
NGC 362	10.5	-1.20	0.4
NGC 288	12.5	-1.27	0.4

Table 4.1: Cluster parameters derived from the isochrone fit

4.2 White Dwarf Cooling Sequence Analysis

I now turn my attention to the main object of this study: the white dwarf luminosity functions of both clusters.

As both clusters are at different distances from Earth, and the reddening coefficients associated with their respective lines-of-sight are also different (if low), a direct comparison of observational magnitudes wouldn't be completely accurate.

Therefore, as in [4], I use the information about each cluster's distance modulus and reddening (found in the literature and confirmed by the isochrone fit above) to derive the *absolute* magnitudes of the white dwarf samples. While the cooling sequence data for NGC 362 reaches slightly deeper, I adopt a single magnitude limit for both clusters and only consider white dwarfs with $M_{F275W} < 9.5$ (see Fig. 4.2).

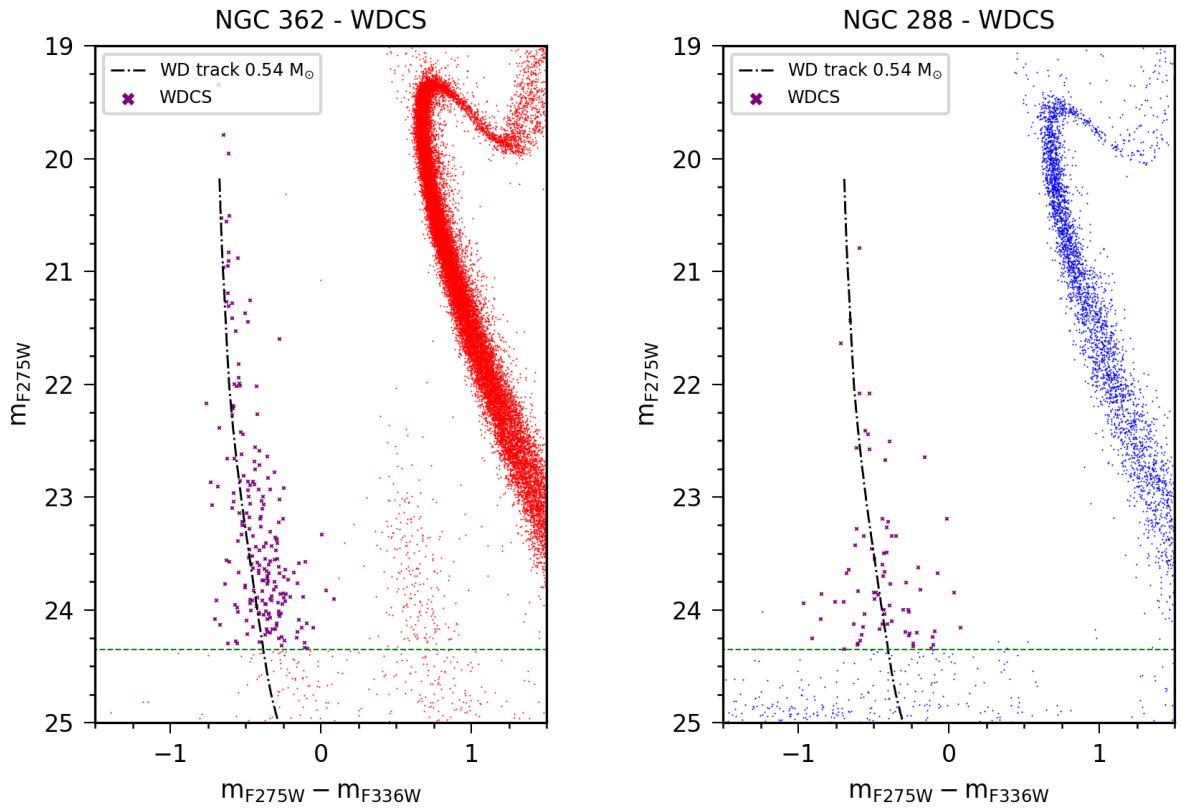

Figure 4.2: The white dwarf samples for both clusters, selected based on proximity to the BaSTI stellar track for a 0.54 $M_{\odot}$ WD and magnitude-limited by the noise floor of NGC 288 (appropriately shifted for the NGC 362 sample).

Due to the large distance from the targets and the high stellar densities in the cores of globular clusters the star counts obtained are inevitably partially incomplete. To account for this, I perform an artificial star test [92] using the routines illustrated in [71] and [54] to derive a completeness estimate for the stars along the WDCS.

The WD counts in the sample, corrected for completeness, can be seen in Fig. 4.3. It should be noted that the completeness fraction for both clusters remains above 0.4 for the entire magnitude interval under consideration. Further details about the Artificial Stars approach to completeness calculation and on its implementation in this work can be found in the Appendix.

Of course, due to both physical differences and observational factors, the number of white dwarfs in the two samples is quite different, and cannot be compared directly. Following the example of Chen *et al.* I adopt a dual approach: for each sequence I calculate a cumulative and a fractional distribution function, normalizing the former by the number of the white dwarfs in each sample, and the latter by the number of RGB stars. The criteria used for RGB star selection are kept as close as possible between the two clusters, with the respective main sequence turn-offs used as

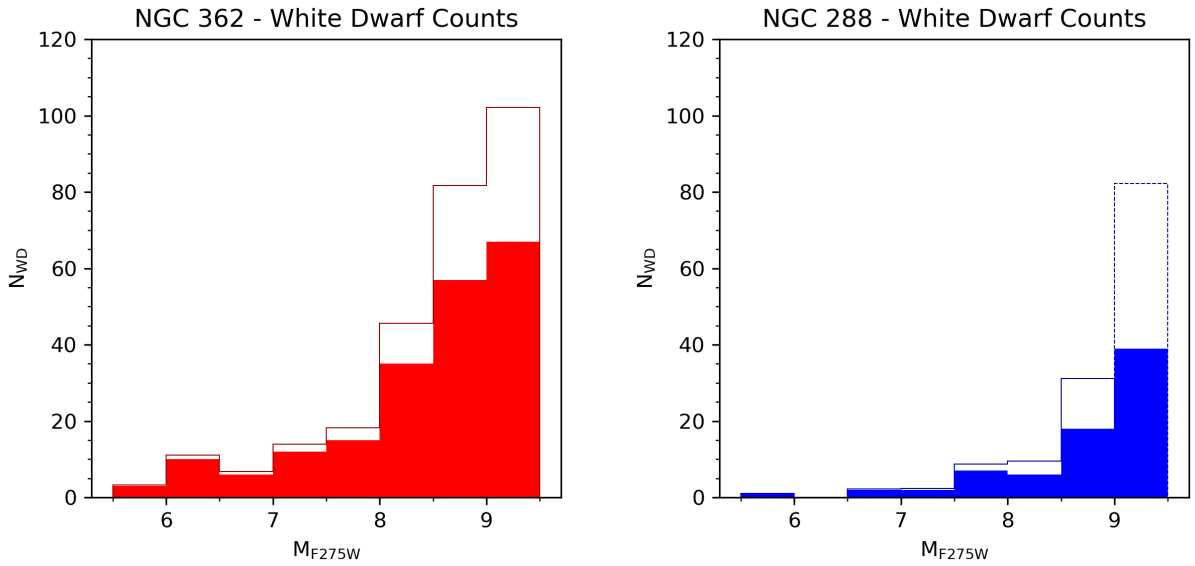

Figure 4.3: Number of WDs in our sample per half-magnitude step for NGC 362 (left) and NGC 288 (right). The bars show the measured counts, while the outlines account for completeness. The dashed outline of the last bin in NGC 288 highlights its low completeness value (below 0.5)

reference[1].

The (completeness-corrected and normalized) fractional luminosity functions can be seen in Fig. 4.4, while the cumulative luminosity function can be seen in Fig. 4.5. As can be seen, in both cases the difference between the two clusters are clear, even if the lower white dwarf and RGB star statistics in my NGC 288 sample are inevitably associated with a significant error. Moreover, the difference in trend seems to resemble that detected by Chen *et al.* between blue-HB clusters M13 and NGC6752, and their second-parameter twins M3 and M5.

4.3 Sampling Bias Analysis

A meaningful comparison of the luminosity functions just obtained for the two clusters relies heavily on the criteria used to both choose our samples and to normalize them. For this reason, as a final step to corroborate the results of this work, I examine the two main factors which could have influenced the analysis:

[1] A few examples of different normalizations will be explored in the next section.

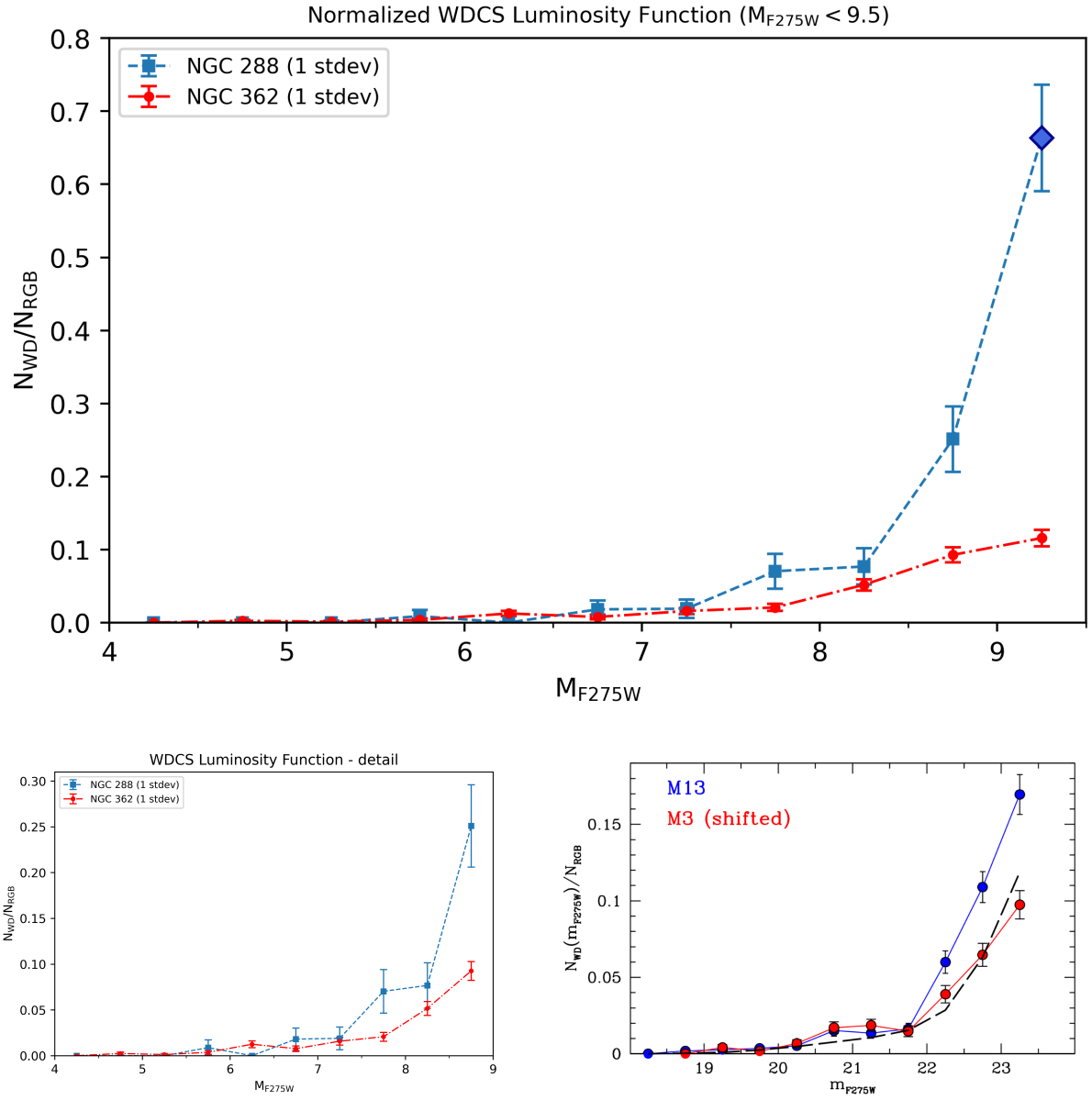

Figure 4.4: *Top:* WDCS luminosity functions for NGC 362 (red circles) and NGC 288 (blue squares) normalized to the number of RGB stars in each cluster. The last, diamond shaped datapoint in the NGC 288 sequence highlights the low completeness leve associated with that magnitude interval. The error bars correspond to one standard deviation. *Bottom left:* zoomed-in detail of the above, limited to $M_{F275W} < 9$. *Bottom right:* the results reported by Chen *et al.* (2021) for M3 and M13 (in relative magnitudes).

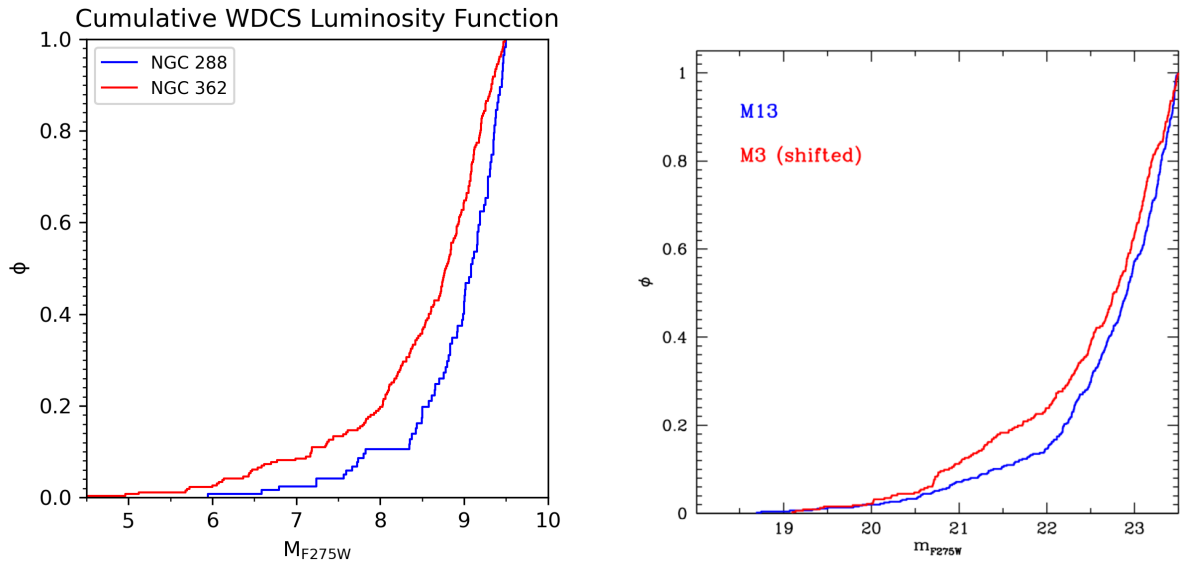

Figure 4.5: On the left: The (completeness-corrected) cumulative WDCS luminosity functions obtained from the sampled white-dwarfs in NGC 362 (red) and NGC 288 (blue), both normalized to the number of sampled WDs in each cluster. On the right, the same functions, calculated by Chen et al. for M3 and M13.

4.3.1 RGB statistics

As WD counts have been normalized with respect to the number of RGB stars in each cluster, it is advisable to check whether might be due not to a variation in the number of hot WDs, but on a non-optimal selection of the RGB sample. To account for this, I recalculate the fractional luminosity functions twice, using the number of sampled HB stars or the MS stars within 1 magnitude from the turn-off as alternative normalization parameters. I find no significant variations in the trends observed, which remain distinct between the two clusters.

Moreover, I note that the NGC 362 and NGC 288 *cumulative* luminosity functions, normalized simply by the total number of cluster WDs sampled, show very similar trends to those of M3 and M13, respectively (see Fig. 4.5).

4.3.2 Dynamical effects

As seen in Chapter 2, the images used in this work cover only the core regions of the two clusters under consideration. Therefore, the possibility that the WD excess in the data might simply be a local artifact should be considered. According to theoretical models, the average WD mass for a cluster similar to NGC 288 is $0.5M_{\odot}$, while the average mass of cluster RGB stars is around $0.7M_{\odot}$, so mass segregation effects could theoretically be at play [93]. However, it must be noted that the portion of the WDCS under examination spans approximately 5 magnitudes, which

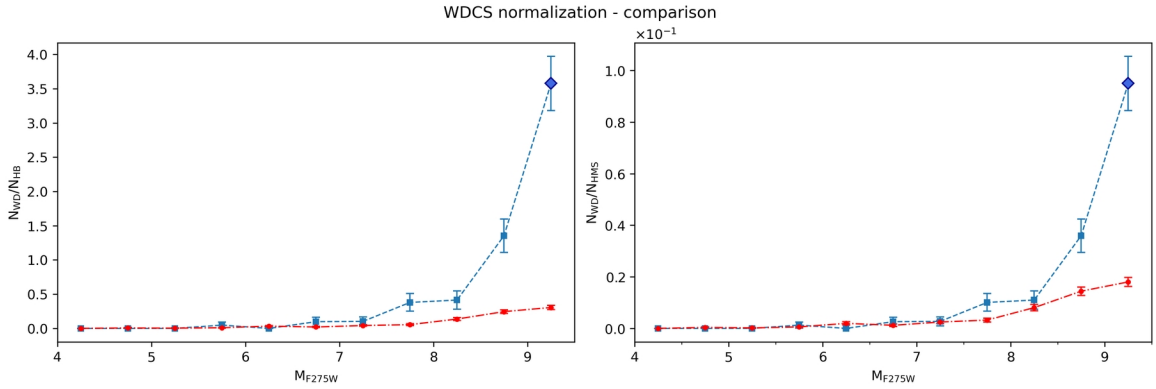

Figure 4.6: The fractional luminosity functions of NGC 362 (red) and NGC 288 (blue) normalized according to two other possible parameters: the number of horizontal branch stars (left) and the number of main sequence stars within 1 magnitude from the turn-off (right). Compare and contrast with Fig. 4.4 and note how, beyond a rescaling factor, the distributions appear virtually unchanged.

corresponds to less than 100 Myrs, a time much smaller than the cluster relaxation time at half mass-radius for both clusters [94].

To confirm this, I divide our RGB and WD samples into two radial bins according to their distance from the cluster center (see Fig. 4.7) and, upon recalculating the luminosity functions separately, still find a significant difference between the WD luminosity functions of the two clusters. The cumulative luminosity distributions, too, only see slight changes with radius.

It is therefore reasonable to assume that dynamical effects such as mass segregation play only a marginal role in the distribution of WDs in the central cluster region.

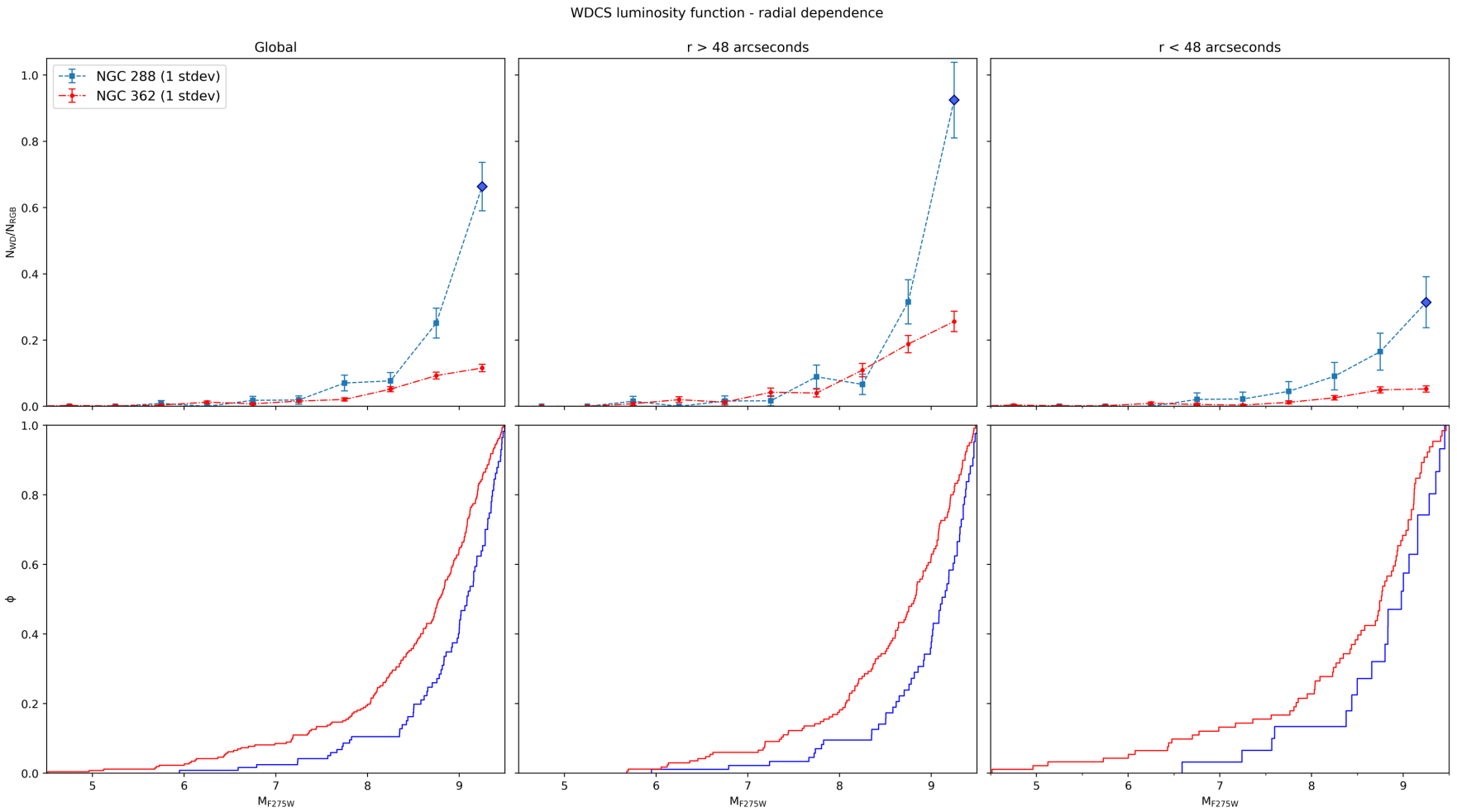

Figure 4.7: A comparison between the luminosity functions of the two cluster cooling sequences calculated (and normalized) according to the number of white dwarfs (and red giant branch stars) in the entire sample (*left*), in the inner 48 arcseconds centered on the cluster core (*center*) and in the outer ring comprising the rest of our data (*right*). While a significant variation can be seen (and the lower counts make for larger relative errors), the difference in trend between the two clusters remains clear.

Chapter 5

Results

Our analysis shows a difference in trend between the white-dwarf luminosity functions of NGC 288 and NGC 362, which bear strong resemblances to those of M13 and M3 respectively, (see Fig. 4.4 and 4.5). In fact, this difference in trend seems noticeably more marked than that detected by Chen *et al.* when considering the $9.5 < M_{F275W} < 10$ magnitude interval [1]. While some of the excess of bright WDs detected in NGC288, *especially* in the aforementioned interval, could be attributed to observational factors such as noise, field contamination and low completeness on the dimmer end of the sequence, it remains significant for a variety of different normalization methods and for different distances from the cluster center (if with notable changes on the dimmer end in the latter case). There is therefore strong evidence that the difference must be physical in nature, and that it might be common to second-parameter cluster pairs.

5.1 Possible Physical Explanations

I therefore explore a number of physical factors which might, alone or in synergy, contribute to explain the observed differences between the cooling sequences examined in both this and previous works:

5.1.1 AGB Manqué Stars

Chen *et al.* report the presence in M13 [2] and NGC 6752 [3] (see also [95]) of a vertical sequence at the blue end of the HB, which they theorize being composed of so called 'AGB *Manqué*' (AGBM) stars - that is, stars which fail to transition to the asymptotic giant branch, instead steadily

[1] Actually, if taken at face value, the difference measured in this interval would be difficult to explain with just the slow cooling model proposed in [3].

increasing in temperature with time before, it is thought, transitioning directly to the white dwarf stage with an hydrogen-rich envelope [96], [97]. Their detection in NGC 288 would therefore support the hypothesis put forward by Chen et al. that these stars are the progenitors of slow-cooling WDs. However, such a sequence cannot be found in either cluster under examination[2]. On one hand, this would mirror the apparent lack of AGBM stars in NGC 6397 [98], which is nonetheless thought to possess slow cooling WDs according to Torres *et al.* [5]. On the other hand, such stars have been identified in NGC 288 by Sahu *et al.* using mid- and far-UV data [99]. Whether or not the detection of these stars is linked to an observed excess of bright white dwarfs remains then uncertain.

5.1.2 Cluster Age

Both the isochrone fit performed in this work and most of the data available in the literature support an age difference of 2-3 Gyrs between NGC 362 and NGC 288. It is therefore natural to consider how age might influence the two cooling sequences. As mentioned in Chapter 1, the age of a stellar population clearly determines both the end and the peak of its white dwarf luminosity function, which progress to higher magnitudes with age. At the same time, the details of WD cooling (such as the reduction in temperature not being linear with age, or more massive white dwarfs cooling more slowly because of their smaller radius and, therefore, radiating surface) determine a slight change in the overall shape of the luminosity function. However, in the time range covered by the magnitude interval under examination (within the first Gyr), the difference shouldn't be significant [12], [20], [44].

On the other hand, there is also an inverse correlation between the age of a cluster and the mass of stars in the horizontal branch. HB stars in an older cluster like NGC 288 would on average have lower mass than those belonging to the sequence in NGC 362, and, according to Althaus *et al.* [8], a larger fraction of them would then be likely to skip the AGB phase and result in slow-burning white dwarfs - this would help explain the differences between the two sequences and, given that cluster age has long been thought a critical factor in shaping HB morphology, also provide additional evidence for it being (one of the) second parameter(s).

5.1.3 Multiple Populations

The discovery, in the last twenty years, of multiple populations in globular clusters has raised numerous questions concerning possible differences in their evolution and their effects on clus-

[2]Except perhaps, for the star at the extreme top left of the NGC 288 single-pass CMD, right above the blue hook. (Fig. 3.1)

ter CMD morphology. For instance, as already mentioned in the introduction, there is evidence for a link between multiple populations and HB morphology, with stars of different groups (and chemical abundances) occupying different positions on the branch. Further evidence comes from the fact that the difference between M3 and M13 clusters - once only based on observations of their horizontal branches, is at least partially reflected by the chemical variations of their "first generation" subpopulations. Furthermore, recent findings support the idea that, in at least 25% of clusters, the distribution of AGB stars is not equal between cluster populations, with a noticeable dearth of "second generation" (or group) stars, who are instead thought to have skipped the sequence entirely and evolved as AGBM ([29] and references therein). Given the theorized correlation between these stars and the existence of slow cooling white dwarfs, the idea that multiple populations could elegantly answer and link together morphology questions ranging from the horizontal branch to the cooling sequence is tempting. However, at present time, there is a lack of both observational evidence linking these phenomena together and of a solid theoretical underpinning for it - for example, according to current astrophysical knowledge and simulations, the measured variations in helium abundance from one population to another are unable to explain the presence of AGBM stars without requiring much higher mass loss in the RGB phase than expected. This hypothesis is, nonetheless, worth investigating.

5.2 Conclusions

To summarize this work:

1. In response to several articles providing evidence of an excess of bright, hot white dwarfs in globular clusters with a blue horizontal branch (such as M13 and NGC 6752) I endeavored to study the white dwarf cooling sequences of the NGC 362/NGC 288 second-parameter cluster pair in order to compare them.

2. Using HST WFC3 data in the F275W and F336W filters, and precision photometry software, we derived the single-pass and multi-pass Color-Magnitude diagrams of the central regions of both clusters. Through isochrone fitting, we obtained estimates for a number of cluster parameters (such as age, metallicity, alpha-enhancement and distance) in broad agreement with the literature.

3. Using the distance modulus and reddening thus found, I retrieved the absolute magnitudes for the cooling sequences of both clusters and, after normalization, compared them, finding a marked difference in the trends of both their cumulative and fractional distribution functions. The difference appears in line with the results obtained by Chen *et al.* for the M3-M13

cluster pair, and even more pronounced at the dimmer end of the magnitude range under consideration.

4. I performed a number of checks aimed at ruling out sampling biases in the results: No significant change (beyond a rescaling) was found when changing the WDCS normalization factor from RGB stars to HB stars or even the stars at the top of the main sequence. When repeating the analysis by dividing the data in two radial bins, the luminosity function of the white dwarfs in the outer section closely mirrored that of the whole cluster, while that of the WDs within 48 arcseconds of the cluster center presented significantly lower values for both clusters in the 9.5-10 M_{F275W} range. The difference in trend between the two clusters appears to still be conserved even in this case, but the uncertainty due to lower statistics complicates this claim. Considering the location and luminosities involved, this might be an effect of incompleteness.

5. I finally explored a number of physical factors which might play a role in the recorded bright WD excess, such as a possible link with AGB-manque stars, the effect of cluster age and the role of multiple stellar populations.

The detection of a bright white dwarf excess in certain clusters - and the search for its causes - is a very recent development: as of the time of writing, the published literature on the topic only covers five clusters - of which only four as part of a comparative analysis between second parameter pairs, and all in the last four years. The theoretical and computational foundations of the slow-cooling hypothesis - the most favored explanation for the excess - have only been established in the past decade. This work then, raising the cluster sample size by 40%, represents a significant contribution to this field, and its results - in alignment with the literature - further add to the available evidence for this phenomenon and its link to the second parameter problem. Nonetheless, it is too early to draw any definite conclusion: not only is the number of cooling sequences examined still very small, but some of the results of this very work (such as the sharp spike in WD numbers for NGC 288 at the faint end of the sampled range, or the variation in trend with radial position - once again most noticeable at the faint end) raise a number of questions. Further analysis of the available data, including a more in-depth study of field contamination, noise and completeness, would address some of these points and refine the existing results. With the data reduction and analysis pipeline thus improved, the study could then be extended to other second-parameter cluster pairs.

Appendix A

Completeness

Any astronomical observation has to deal with the fact that, due to instrumental reasons (e.g. sensitivity limitations, noise) or physical ones (such as simple line of sight and perspective), it can seldom capture *every* object in the field of view. The fraction of detected objects (in this case, stars) over the amount of expected ones is called the *completeness* of the sample. Due to the physical and observational origins of incompleteness, the detected stars are not a perfectly random sample of the population: this adds a degree of uncertainty to any statistical data gained from the sample - a bias that must be estimated and accounted for.

A.1 Artificial Stars

Completeness can be estimated through a number of theoretical methods, such as Confusion calculation and luminosity function analysis, all of which have a number of limitations due to the need for a number of starting assumptions (see e.g. [100] and further references therein). However, another very common method of completeness estimation is empirical, and makes use of so-called 'artificial stars' as, for example, in [101] or, more recently, in [102].

The principle of the method is simple: a number of software-generated star-like flux peaks of random (within preset parameters) position and intensity are generated, recorded, then added to the initial image. The modified image is then analyzed with the same criteria used for the original. At the end of the reduction pipeline, the resulting stellar catalogue is confronted with the artificial star list and any matches recorded. The number of artificial stars who are thus recovered are then used to estimate completeness by way of the ratio:

$$C = N^{AS}_{Recovered} / N^{AS}_{Total} \tag{A.1}$$

In practice, the situation is significantly more complex: due to the aforementioned physical and observational factors, the degree of completeness within an image depends on both the number density of the stars in a given area and on the magnitude considered, requiring multiple specific runs to obtain a precise, sufficiently granular estimate. Moreover, the stochastic nature of the test requires a high number of artificial sources to achieve satisfactory accuracy, which can be a significant fraction of the *actual* stars in the image - distorting the measurement by introducing artificial crowding. This problem can be partially mitigated by accepting a lower number of artificial stars and requiring them to be generated at a minimum distance from each other or, alternatively, sidestepped by *serializing* the process in multiple smaller batches, albeit at increased computational cost.

A.2 Cluster WDCS completeness

While analyzing the dataset in this work, I employed the artificial stars method to calculate its completeness. Due to computational power and time constraints, this analysis was restricted to the main objects of interests, the WDCSs of both clusters.

The method chosen was very close to that used in [54]: $3{\cdot}10^5$ artificial stars were generated for each cluster, with magnitude and color ranges matching those of the respective cooling sequences and giant branches. I adopted a flat luminosity distribution in the F275W magnitude and a similarly flat spatial distribution, which is an acceptable approximation in this case as the images used only probe the high-density cluster cores. Following a novel method pioneered by Anderson *et al.* [71], each artificial star was added to a *different* copy of the base image. All the thus modified copies (with a single artificial star each) were then individually reduced with the same data pipeline, algorithms and selection criteria used for the original images. While very computationally intensive, this approach eliminated the risk of self-interference between artificial stars. The number of artificial stars recovered at the end of this procedure was then used to calculate the recovery efficiency: as this quantity depends on both stellar luminosity and crowding we calculated the WD recovery fraction for 12 half-magnitude values in the $4.0 < M_{F275W} < 10$ range, and interpolated those datapoints to assign a completeness value to each white dwarf in our samples. As can be seen from Fig. A.1, the completeness values for both cooling sequences are quite high for brighter stars but, as expected, degrade with magnitude, and more so for NGC 288 than for NGC 362, introducing a significant correction to the white-dwarf counts on the lower end. In particular, completeness for the former drops below 0.5 for the $9.5 < M_{F275W} < 10$ magnitude interval - which suggests some caution should be taken when analyzing star counts in this range. In any case, the completeness value remains above 0.4 for both clusters in the entire magnitude range considered.

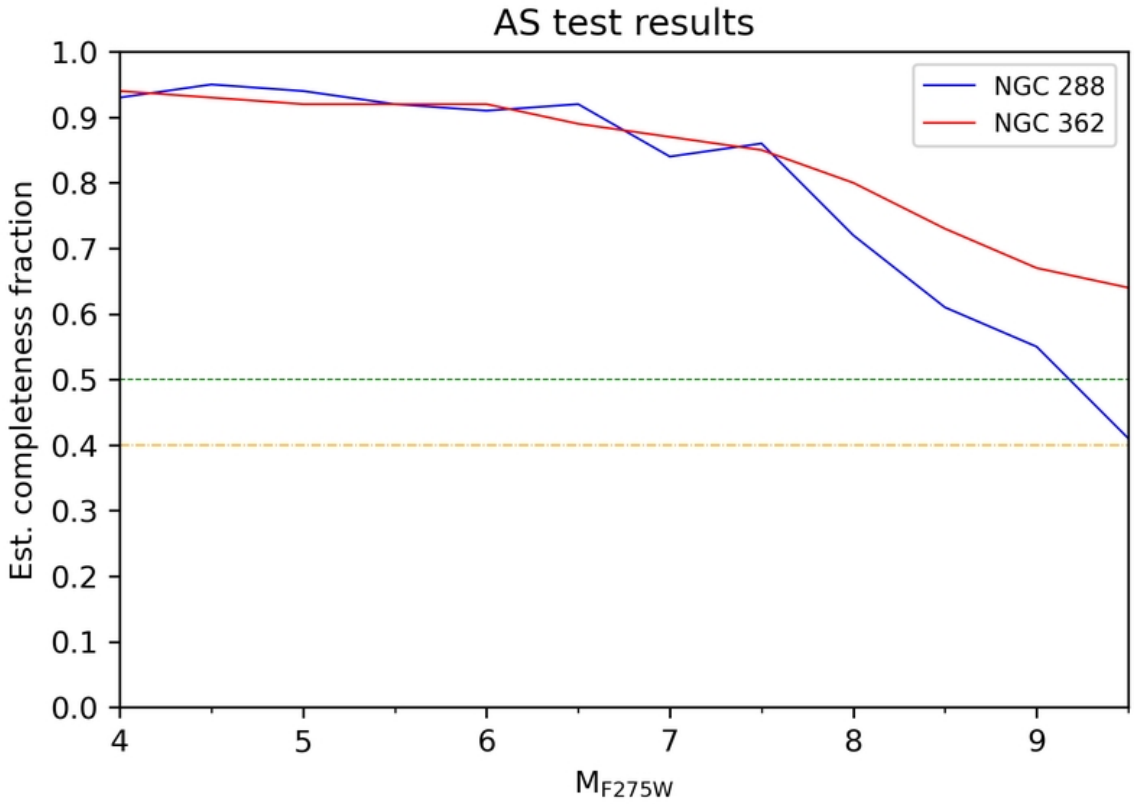

Figure A.1: Artificial star test results: completeness fraction estimate as a function of magnitude (M_{F275W}) for the white dwarfs in NGC 362 (red) and NGC 288 (blue).

Bibliography

[1] D. Saumon, S. Blouin, and P.-E. Tremblay, "Current challenges in the physics of white dwarf stars," *Physics Reports*, vol. 988, pp. 1–63, 2022, Current Challenges in the Physics of White Dwarf Stars, ISSN: 0370-1573. DOI: https://doi.org/10.1016/j.physrep.2022.09.001. [Online]. Available: https://www.sciencedirect.com/science/article/pii/S0370157322003180.

[2] J. Chen, F. R. Ferraro, M. Cadelano, *et al.*, "Slowly cooling white dwarfs in M13 from stable hydrogen burning," *Nature Astronomy*, vol. 5, pp. 1170–1177, Nov. 2021. DOI: 10.1038/s41550-021-01445-6. arXiv: 2109.02306 [astro-ph.GA].

[3] J. Chen, F. R. Ferraro, M. Cadelano, *et al.*, "Slowly Cooling White Dwarfs in NGC 6752," ApJ, vol. 934, no. 2, 93, p. 93, Aug. 2022. DOI: 10.3847/1538-4357/ac7a45. arXiv: 2206.10039 [astro-ph.SR].

[4] J. Chen, F. R. Ferraro, M. Salaris, *et al.*, "The "Canonical" White Dwarf Cooling Sequence of M5," ApJ, vol. 950, no. 2, 155, p. 155, Jun. 2023. DOI: 10.3847/1538-4357/acd173. arXiv: 2304.14847 [astro-ph.SR].

[5] S. Torres, E. García-Berro, L. G. Althaus, and M. E. Camisassa, "The white dwarf population of NGC 6397," A&A, vol. 581, A90, A90, Sep. 2015. DOI: 10.1051/0004-6361/201526157. arXiv: 1507.08806 [astro-ph.GA].

[6] G. A. Gontcharov, C. J. Bonatto, O. S. Ryutina, *et al.*, "Isochrone fitting of Galactic globular clusters - V. NGC 6397 and NGC 6809 (M55)," MNRAS, vol. 526, no. 4, pp. 5628–5647, Dec. 2023. DOI: 10.1093/mnras/stad3134. arXiv: 2402.06524 [astro-ph.GA].

[7] M. Miller Bertolami, L. Althaus, and E. Garcia-Berro, "Quiescent nuclear burning in low-metallicity white dwarfs," *The Astrophysical Journal Letters*, vol. 775, Aug. 2013. DOI: 10.1088/2041-8205/775/1/L22.

[8] L. G. Althaus, M. E. Camisassa, M. M. M. Bertolami, A. H. C'orsico, and E. Garc'ia-Berro, "White dwarf evolutionary sequences for low-metallicity progenitors: The impact of third dredge-up," *Astronomy and Astrophysics*, vol. 576, pp. 1–11, 2015. [Online]. Available: https://api.semanticscholar.org/CorpusID:31740446.

[9] I. Renedo, L. G. Althaus, M. M. Miller Bertolami, *et al.*, "New Cooling Sequences for Old White Dwarfs," ApJ, vol. 717, no. 1, pp. 183–195, Jul. 2010. DOI: 10.1088/0004-637X/717/1/183. arXiv: 1005.2170 [astro-ph.SR].

[10] J. B. Holberg, "How Degenerate Stars Came to be Known as White Dwarfs," in *American Astronomical Society Meeting Abstracts*, ser. American Astronomical Society Meeting Abstracts, vol. 207, Dec. 2005, 205.01, p. 205.01.

[11] Gaia Collaboration, R. L. Smart, L. M. Sarro, *et al.*, "Gaia Early Data Release 3. The Gaia Catalogue of Nearby Stars," A&A, vol. 649, A6, A6, May 2021. DOI: 10.1051/0004-6361/202039498. arXiv: 2012.02061 [astro-ph.SR].

[12] G. Fontaine, P. Brassard, and P. Bergeron, "The Potential of White Dwarf Cosmochronology," PASP, vol. 113, no. 782, pp. 409–435, Apr. 2001. DOI: 10.1086/319535.

[13] J. Liebert, P. Bergeron, D. Eisenstein, *et al.*, "A helium white dwarf of extremely low mass," *The Astrophysical Journal*, vol. 606, no. 2, p. L147, Apr. 2004. DOI: 10.1086/421462. [Online]. Available: https://dx.doi.org/10.1086/421462.

[14] K. Werner, N. J. Hammer, T. Nagel, T. Rauch, and S. Dreizler, "On Possible Oxygen/Neon White Dwarfs: H1504+65 and the White Dwarf Donors in Ultracompact X-ray Binaries," in *14th European Workshop on White Dwarfs*, D. Koester and S. Moehler, Eds., ser. Astronomical Society of the Pacific Conference Series, vol. 334, Jul. 2005, p. 165. DOI: 10.48550/arXiv.astro-ph/0410690. arXiv: astro-ph/0410690 [astro-ph].

[15] P.-E. Tremblay, G. Fontaine, N. P. Gentile Fusillo, *et al.*, "Core crystallization and pile-up in the cooling sequence of evolving white dwarfs," Nature, vol. 565, no. 7738, pp. 202–205, Jan. 2019. DOI: 10.1038/s41586-018-0791-x. arXiv: 1908.00370 [astro-ph.SR].

[16] L. Mestel, "On the Theory of White Dwarf Stars: I. The Energy Sources of White Dwarfs," *Monthly Notices of the Royal Astronomical Society*, vol. 112, no. 6, pp. 583–597, Dec. 1952, ISSN: 0035-8711. DOI: 10.1093/mnras/112.6.583. eprint: https://academic.oup.com/mnras/article-pdf/112/6/583/8077605/mnras112-0583.pdf. [Online]. Available: https://doi.org/10.1093/mnras/112.6.583.

[17] M. Salaris, S. Cassisi, A. Pietrinferni, P. M. Kowalski, and J. Isern, "A large stellar evolution database for population synthesis studies. vi. white dwarf cooling sequences," *The Astrophysical Journal*, vol. 716, pp. 1241 –1251, 2010. [Online]. Available: https://api.semanticscholar.org/CorpusID:44236134.

[18] M. Schmidt, "The Rate of Star Formation.," ApJ, vol. 129, p. 243, Mar. 1959. DOI: 10.1086/146614.

[19] H. M. van Horn, "Cooling of White Dwarfs," in *White Dwarfs*, W. J. Luyten, Ed., vol. 42, Jan. 1971, p. 97.

[20] M. Salaris, "White dwarf cosmochronology: Techniques and uncertainties," *Proceedings of The International Astronomical Union*, vol. 258, pp. 287–298, Oct. 2009. DOI: 10.1017/S1743921309031937.

[21] J. Iben I. and J. MacDonald, "The effects of diffusion due to gravity and due to composition gradients on the rate of hydrogen burning in a cooling degenerate dwarf. I - The case of a thick helium buffer layer," ApJ, vol. 296, pp. 540–553, Sep. 1985. DOI: 10.1086/163473.

[22] J. Iben I. and J. MacDonald, "The Effects of Diffusion Due to Gravity and Due to Composition Gradients on the Rate of Hydrogen Burning in a Cooling Degenerate Dwarf. II. Dependence on Initial Metallicity and on Buffer Mass," ApJ, vol. 301, p. 164, Feb. 1986. DOI: 10.1086/163884.

[23] M. M. M. Bertolami, L. G. Althaus, and E. García–Berro, "Quiescent nuclear burning in low-metallicity white dwarfs," *The Astrophysical Journal Letters*, vol. 775, 2013. [Online]. Available: https://api.semanticscholar.org/CorpusID:118659325.

[24] *The Harlow Shapley Symposium on Globular Cluster Systems in Galaxies: proceedings of the 126th symposium of the International Astronomical Union, held in Cambridge, Massachusetts, U.S.A. August 25-29, 1986.* Vol. 126, Jan. 1988.

[25] A. R. Sandage, "The color-magnitude diagram for the globular cluster M 3.," AJ, vol. 58, pp. 61–75, Jan. 1953. DOI: 10.1086/106822.

[26] R. Gratton, A. Bragaglia, E. Carretta, V. D'Orazi, S. Lucatello, and A. Sollima, "What is a globular cluster? an observational perspective," *The Astronomy and Astrophysics Review*, vol. 27, pp. 1–136, 2019. [Online]. Available: https://api.semanticscholar.org/CorpusID:207847491.

[27] J. S. Kalirai and H. B. Richer, "Star clusters as laboratories for stellar and dynamical evolution," *Philosophical Transactions of the Royal Society A: Mathematical, Physical and Engineering Sciences*, vol. 368, no. 1913, pp. 755–782, 2010. DOI: 10.1098/rsta.2009.0257. eprint: https://royalsocietypublishing.org/doi/pdf/10.1098/rsta.2009.0257. [Online]. Available: https://royalsocietypublishing.org/doi/abs/10.1098/rsta.2009.0257.

[28] J. Anderson, L. R. Bedin, G. Piotto, R. S. Yadav, and A. Bellini, "Ground-based CCD astrometry with wide field imagers. I. Observations just a few years apart allow decontamination of field objects from members in two globular clusters," A&A, vol. 454, no. 3, pp. 1029–1045, Aug. 2006. DOI: 10.1051/0004-6361:20065004. arXiv: astro-ph/0604541 [astro-ph].

[29] A. P. Milone and A. F. Marino, "Multiple Populations in Star Clusters," *Universe*, vol. 8, no. 7, 359, p. 359, Jun. 2022. DOI: 10.3390/universe8070359. arXiv: 2206.10564 [astro-ph.GA].

[30] H. C. Arp, W. A. Baum, and A. R. Sandage, "The HR diagrams for the globular clusters M 92 and M 3.," AJ, vol. 57, pp. 4–5, Apr. 1952. DOI: 10.1086/106674.

[31] M. Catelan, "Horizontal Branch Stars and the Ultraviolet Universe," in *New Quests in Stellar Astrophysics. II. Ultraviolet Properties of Evolved Stellar Populations*, ser. Astrophysics and Space Science Proceedings, vol. 7, Mar. 2009, pp. 175–189. DOI: 10.1007/978-0-387-87621-4_27. arXiv: 0708.2445 [astro-ph].

[32] R. Kippenhahn, A. Weigert, and A. Weiss, *Stellar Structure and Evolution* (Astronomy and Astrophysics Library). Springer Berlin Heidelberg, 2012, ISBN: 9783642303043. [Online]. Available: https://books.google.it/books?id=wdSFB4B_pMUC.

[33] A. Sandage and G. Wallerstein, "Color-Magnitude Diagram for Disk Globular Cluster NGC 6356 Compared with Halo Clusters.," ApJ, vol. 131, p. 598, May 1960. DOI: 10.1086/146872.

[34] S. van den Bergh, "UBV photometry of globular clusters.," AJ, vol. 72, pp. 70–81, Feb. 1967. DOI: 10.1086/110203.

[35] A. L. Dotter, A. Sarajedini, J. Anderson, *et al.*, "The acs survey of galactic globular clusters. ix. horizontal branch morphology and the second parameter phenomenon," *The Astrophysical Journal*, vol. 708, pp. 698 –716, 2009. [Online]. Available: https://api.semanticscholar.org/CorpusID:16374358.

[36] A. L. Dotter, "The second parameter problem(s)," 2013. [Online]. Available: https://api.semanticscholar.org/CorpusID:59500511.

[37] A. F. Marino, A. P. Milone, and K. Lind, "Horizontal branch morphology and multiple stellar populations in the anomalous globular cluster m 22*," *The Astrophysical Journal*, vol. 768, no. 1, p. 27, Apr. 2013. DOI: 10.1088/0004-637X/768/1/27. [Online]. Available: https://dx.doi.org/10.1088/0004-637X/768/1/27.

[38] R. G. Gratton, S. Lucatello, A. Sollima, *et al.*, "The Na-O anticorrelation in horizontal branch stars. III. 47 Tucanae and M 5," A&A, vol. 549, A41, A41, Jan. 2013. DOI: 10.1051/0004-6361/201219976. arXiv: 1210.4069 [astro-ph.SR].

[39] L. Lovisi, A. Mucciarelli, B. Lanzoni, *et al.*, "Chemical and Kinematical Properties of Blue Straggler Stars and Horizontal Branch Stars in NGC 6397," ApJ, vol. 754, no. 2, 91, p. 91, Aug. 2012. DOI: 10.1088/0004-637X/754/2/91. arXiv: 1205.5561 [astro-ph.SR].

[40] B. Hansen, J. Anderson, J. P. Brewer, *et al.*, "The white dwarf cooling sequence of ngc 6397," *The Astrophysical Journal*, vol. 671, pp. 380 –401, 2005. [Online]. Available: https://api.semanticscholar.org/CorpusID:119419597.

[41] L. R. Bedin, M. Salaris, I. R. King, G. Piotto, J. Anderson, and S. Cassisi, "The bottom of the white dwarf cooling sequence in the old open cluster ngc 2158*," *The Astrophysical Journal Letters*, vol. 708, no. 1, p. L32, Dec. 2009. DOI: 10.1088/2041-8205/708/1/L32. [Online]. Available: https://dx.doi.org/10.1088/2041-8205/708/1/L32.

[42] A. Bellini, L. Bedin, G. Piotto, *et al.*, "The end of the white dwarf cooling sequence in m 67," English (US), *Astronomy and Astrophysics*, vol. 513, no. 10, Apr. 2010, ISSN: 0004-6361. DOI: 10.1051/0004-6361/200913721.

[43] L. Bedin, M. Salaris, J. Anderson, *et al.*, "The hst large programme on ngc 6752 – iv. the white dwarf sequence," English (US), *Monthly Notices of the Royal Astronomical Society*, vol. 518, no. 3, pp. 3722–3736, Jan. 2023, Publisher Copyright: © 2022 The Author(s) Published by Oxford University Press on behalf of Royal Astronomical Society., ISSN: 0035-8711. DOI: 10.1093/mnras/stac3219.

[44] M. Salaris, L. G. Althaus, and E. Garc'ia-Berro, "Comparison of theoretical white dwarf cooling timescales," *Astronomy and Astrophysics*, vol. 555, 2013. [Online]. Available: https://api.semanticscholar.org/CorpusID:28498561.

[45] D. A. VandenBerg, K. Brogaard, R. Leaman, and L. Casagrande, "The ages of 55 globular clusters as determined using an improved method along with color–magnitude diagram constraints, and their implications for broader issues," *The Astrophysical Journal*, vol. 775, 2013. [Online]. Available: https://api.semanticscholar.org/CorpusID:117065283.

[46] M. Catelan, M. Bellazzini, W. B. Landsman, *et al.*, "Age as the second parameter in ngc 288/ngc 362? ii. the horizontal branch revisited," *The Astronomical Journal*, vol. 122, pp. 3171 –3182, 2001. [Online]. Available: https://api.semanticscholar.org/CorpusID:7494.

[47] M. J. Bolte, "The age of the globular cluster ngc 288, the formation of the galactic halo, and the second parameter," *The Astronomical Journal*, vol. 97, p. 1688, 1989. [Online]. Available: https://api.semanticscholar.org/CorpusID:122856522.

[48] A. Sarajedini and P. Demarque, "A new age diagnostic applied to the globular clusters ngc 288 and ngc 362," *The Astrophysical Journal*, vol. 365, pp. 219–223, 1990. [Online]. Available: https://api.semanticscholar.org/CorpusID:121821392.

[49] S. P. Caldwell and R. J. Dickens, "Chemical abundances in the globular clusters NGC 288, NGC 362, NGC 6397 and M 55.," MNRAS, vol. 234, pp. 87–94, Sep. 1988. DOI: 10.1093/mnras/234.1.87.

[50] A. Sarajedini, "Relative and absolute ages of Galactic globular clusters," in *The Ages of Stars*, E. E. Mamajek, D. R. Soderblom, and R. F. G. Wyse, Eds., vol. 258, Jun. 2009, pp. 221–232. DOI: 10.1017/S1743921309031871.

[51] D. A. VandenBerg and P. R. Durrell, "Is age really the second parameter in globular clusters," *The Astronomical Journal*, vol. 99, p. 221, 1990. [Online]. Available: https://api.semanticscholar.org/CorpusID:121528307.

[52] D. E. McLaughlin and R. P. van der Marel, "Resolved massive star clusters in the milky way and its satellites: Brightness profiles and a catalog of fundamental parameters," *The Astrophysical Journal Supplement Series*, vol. 161, pp. 304 –360, 2005. [Online]. Available: https://api.semanticscholar.org/CorpusID:18814794.

[53] M. Libralato, A. Bellini, R. P. van der Marel, *et al.*, "Hubble space telescope proper motion (hstpromo) catalogs of galactic globular cluster. vi. improved data reduction and internal-kinematic analysis of ngc 362," *The Astrophysical Journal*, vol. 861, 2018. [Online]. Available: https://api.semanticscholar.org/CorpusID:119491333.

[54] A. Milone, G. Piotto, L. Bedin, *et al.*, "The acs survey of galactic globular clusters. xii. photometric binaries along the main-sequence," *Astronomy and Astrophysics*, vol. 540, Nov. 2011. DOI: 10.1051/0004-6361/201016384.

[55] F. Ferraro, B. Paltrinieri, F. F. Pecci, *et al.*, "Hst uv observations of the cores of m3 and m13," *arXiv: Astrophysics*, 1997. [Online]. Available: https://api.semanticscholar.org/CorpusID:18641453.

[56] V. Caloi and F. D'Antona, "Helium self-enrichment in globular clusters and the second parameter problem in m 3 and m 13," *Astronomy and Astrophysics*, vol. 435, pp. 987–993, 2005. [Online]. Available: https://api.semanticscholar.org/CorpusID:2999640.

[57] A. P. Milone, G. Piotto, A. Renzini, *et al.*, "The Hubble Space Telescope UV Legacy Survey of Galactic globular clusters - IX. The Atlas of multiple stellar populations," MNRAS, vol. 464, no. 3, pp. 3636–3656, Jan. 2017. DOI: 10.1093/mnras/stw2531. arXiv: 1610.00451 [astro-ph.SR].

[58] D. J. Schlegel, D. P. Finkbeiner, and M. Davis, "Maps of Dust Infrared Emission for Use in Estimation of Reddening and Cosmic Microwave Background Radiation Foregrounds," ApJ, vol. 500, no. 2, pp. 525–553, Jun. 1998. DOI: 10.1086/305772. arXiv: astro-ph/9710327 [astro-ph].

[59] E. F. Schlafly and D. P. Finkbeiner, "Measuring Reddening with Sloan Digital Sky Survey Stellar Spectra and Recalibrating SFD," ApJ, vol. 737, no. 2, 103, p. 103, Aug. 2011. DOI: 10.1088/0004-637X/737/2/103. arXiv: 1012.4804 [astro-ph.GA].

[60] G. Piotto, A. P. Milone, L. R. Bedin, *et al.*, "The Hubble Space Telescope UV Legacy Survey of Galactic Globular Clusters. I. Overview of the Project and Detection of Multiple Stellar Populations," AJ, vol. 149, no. 3, 91, p. 91, Mar. 2015. DOI: 10.1088/0004-6256/149/3/91. arXiv: 1410.4564 [astro-ph.SR].

[61] G. Piotto, A. P. Milone, A. P. Milone, *et al.*, "Multi-wavelength hubble space telescope photometry of stellar populations in ngc 288," *The Astrophysical Journal*, vol. 775, 2013. [Online]. Available: https://api.semanticscholar.org/CorpusID:118584865.

[62] J. Kalirai, M. Correnti, J. Cummings, *et al.*, *Using Stellar Evolution as a Clock to Watch the Dynamical Evolution of a Globular Cluster*, HST Proposal. Cycle 23, ID. #14155, Dec. 2016.

[63] K. Sahu, "WFC3 Data Handbook v. 5," in *WFC3 Data Handbook v. 5*, vol. 5, 2021, p. 5.

[64] J. Anderson and L. R. Bedin, "An Empirical Pixel-Based Correction for Imperfect CTE. I. HST's Advanced Camera for Surveys," PASP, vol. 122, no. 895, p. 1035, Sep. 2010. DOI: 10.1086/656399. arXiv: 1007.3987 [astro-ph.IM].

[65] D. Nardiello, M. Libralato, G. Piotto, *et al.*, "The Hubble Space Telescope UV Legacy Survey of Galactic Globular Clusters - XVII. Public Catalogue Release," MNRAS, vol. 481, no. 3, pp. 3382–3393, Dec. 2018. DOI: 10.1093/mnras/sty2515. arXiv: 1809.04300 [astro-ph.SR].

[66] Milone, A. P., Cordoni, G., Marino, A. F., *et al.*, "Hubble space telescope survey of magellanic cloud star clusters - photometry and astrometry of 113 clusters and early results⋆," *AA*, vol. 672, A161, 2023. DOI: 10.1051/0004-6361/202244798. [Online]. Available: https://doi.org/10.1051/0004-6361/202244798.

[67] C. R. Harris, K. J. Millman, S. J. van der Walt, *et al.*, "Array programming with NumPy," *Nature*, vol. 585, no. 7825, pp. 357–362, Sep. 2020. DOI: 10.1038/s41586-020-2649-2. [Online]. Available: https://doi.org/10.1038/s41586-020-2649-2.

[68] Wes McKinney, "Data Structures for Statistical Computing in Python," in *Proceedings of the 9th Python in Science Conference*, Stéfan van der Walt and Jarrod Millman, Eds., 2010, pp. 56 –61. DOI: 10.25080/Majora-92bf1922-00a.

[69] A. Bellini, G. Piotto, A. Milone, *et al.*, "The intriguing stellar populations in the globular clusters ngc 6388 and ngc 6441," *The Astrophysical Journal*, vol. 765, Jan. 2013. DOI: 10.1088/0004-637X/765/1/32.

[70] J. Anderson and I. R. King, "Toward High-Precision Astrometry with WFPC2. I. Deriving an Accurate Point-Spread Function," PASP, vol. 112, no. 776, pp. 1360–1382, Oct. 2000. DOI: 10.1086/316632. arXiv: astro-ph/0006325 [astro-ph].

[71] J. Anderson, A. Sarajedini, L. R. Bedin, *et al.*, "The Acs Survey of Globular Clusters. V. Generating a Comprehensive Star Catalog for each Cluster," AJ, vol. 135, no. 6, pp. 2055–2073, Jun. 2008. DOI: 10.1088/0004-6256/135/6/2055. arXiv: 0804.2025 [astro-ph].

[72] R. L. Gilliland, A. Rajan, and S. E. Deustua, "Wfc3 uvis full well depths, and linearity near and beyond saturation," 2010. [Online]. Available: https://api.semanticscholar.org/CorpusID:14507815.

[73] A. Bellini and L. R. Bedin, "Astrometry and photometry with hst wfc3. i. geometric distortion corrections of f225w, f275w, f336w bands of the uvis channel," *Publications of the Astronomical Society of the Pacific*, vol. 121, no. 886, pp. 1419–1428, 2009, ISSN: 00046280, 15383873. [Online]. Available: http://www.jstor.org/stable/10.1086/649061 (visited on 03/03/2024).

[74] A. Bellini, J. Anderson, and L. R. Bedin, "Astrometry and Photometry with HST WFC3. II. Improved Geometric-Distortion Corrections for 10 Filters of the UVIS Channel," PASP, vol. 123, no. 903, p. 622, May 2011. DOI: 10.1086/659878. arXiv: 1102.5218 [astro-ph.IM].

[75] Gaia Collaboration, A. G. A. Brown, A. Vallenari, *et al.*, "Gaia Early Data Release 3. Summary of the contents and survey properties," A&A, vol. 649, A1, A1, May 2021. DOI: 10.1051/0004-6361/202039657. arXiv: 2012.01533 [astro-ph.GA].

[76] R. C. Bohlin, I. Hubeny, and T. Rauch, "New Grids of Pure-hydrogen White Dwarf NLTE Model Atmospheres and the HST/STIS Flux Calibration," AJ, vol. 160, no. 1, 21, p. 21, Jul. 2020. DOI: 10.3847/1538-3881/ab94b4. arXiv: 2005.10945 [astro-ph.SR].

[77] A. Calamida, J. Mack, J. Medina, *et al.*, "New time-dependent wfc3 uvis inverse sensitivities," 2021. [Online]. Available: https://api.semanticscholar.org/CorpusID:259257409.

[78] M. Bellazzini, F. F. Pecci, M. Messineo, L. Monaco, and R. T. Rood, "Deep hubble space telescope wfpc2 photometry of ngc 288. i. binary systems and blue stragglers," *The Astronomical Journal*, vol. 123, pp. 1509 –1527, 2001. [Online]. Available: https://api.semanticscholar.org/CorpusID:15755134.

[79] D.-G. Roh, Y.-W. Lee, S.-J. Joo, S.-I. Han, Y.-J. Sohn, and J.-W. Lee, "Two distinct red giant branches in the globular cluster ngc 288," *The Astrophysical Journal Letters*, vol. 733, no. 2, p. L45, May 2011. DOI: 10.1088/2041-8205/733/2/L45. [Online]. Available: https://dx.doi.org/10.1088/2041-8205/733/2/L45.

[80] G. Piotto, G. Piotto, A. P. Milone, *et al.*, "Multi-wavelength hubble space telescope photometry of stellar populations in ngc 288," *The Astrophysical Journal*, vol. 775, 2013. [Online]. Available: https://api.semanticscholar.org/CorpusID:118584865.

[81] E. Carretta, A. Bragaglia, R. Gratton, *et al.*, "Ngc 362: Another globular cluster with a split red giant branch," *Astronomy and Astrophysics*, vol. 557, Jul. 2013. DOI: 10.1051/0004-6361/201321905.

[82] E. Sabbi, D. J. Lennon, J. Anderson, *et al.*, "Hubble Tarantula Treasury Project. III. Photometric Catalog and Resulting Constraints on the Progression of Star Formation in the 30 Doradus Region," ApJS, vol. 222, no. 1, 11, p. 11, May 2016. DOI: 10.3847/0067-0049/222/1/11. arXiv: 1511.06021 [astro-ph.GA].

[83] A. Bellini, J. Anderson, L. R. Bedin, *et al.*, "The State-of-the-art HST Astro-photometric Analysis of the Core of ω Centauri. I. The Catalog," ApJ, vol. 842, no. 1, 6, p. 6, Jun. 2017. DOI: 10.3847/1538-4357/aa7059. arXiv: 1704.07425 [astro-ph.SR].

[84] L. R. Bedin, I. R. King, J. Anderson, *et al.*, "Reaching the end of the white dwarf cooling sequence in ngc 6791*," *The Astrophysical Journal*, vol. 678, no. 2, p. 1279, May 2008. DOI: 10.1086/529370. [Online]. Available: https://dx.doi.org/10.1086/529370.

[85] A. Pietrinferni, S. Cassisi, M. Salaris, and F. Castelli, "A large stellar evolution database for population synthesis studies. i. scaled solar models and isochrones," *The Astrophysical Journal*, vol. 612, pp. 168 –190, 2004. [Online]. Available: https://api.semanticscholar.org/CorpusID:18033676.

[86] A. Pietrinferni, S. Cassisi, M. Salaris, and F. Castelli, "A large stellar evolution database for population synthesis studies. ii. stellar models and isochrones for an α-enhanced metal distribution," *The Astrophysical Journal*, vol. 642, pp. 797 –812, 2006. [Online]. Available: https://api.semanticscholar.org/CorpusID:17314319.

[87] A. Pietrinferni, S. L. Hidalgo, S. Cassisi, *et al.*, "The updated basti stellar evolution models and isochrones: Ii. alpha-enhanced calculations," 2020. [Online]. Available: https://api.semanticscholar.org/CorpusID:229332082.

[88] G. A. Gontcharov, M. Y. Khovritchev, A. V. Mosenkov, *et al.*, "Isochrone fitting of galactic globular clusters – iii. ngc 288, ngc 362, and ngc 6218 (m12)," *Monthly Notices of the Royal Astronomical Society*, 2021. [Online]. Available: https://api.semanticscholar.org/CorpusID:237940433.

[89] Carretta, E., Bragaglia, A., Gratton, R. G., *et al.*, "Ngc 362: Another globular cluster with a split red giant branch," *AA*, vol. 557, A138, 2013. DOI: 10.1051/0004-6361/201321905. [Online]. Available: https://doi.org/10.1051/0004-6361/201321905.

[90] M. Catelan, M. Bellazzini, W. B. Landsman, *et al.*, "Age as the second parameter in ngc 288/ngc 362? ii. the horizontal branch revisited," *The Astronomical Journal*, vol. 122, pp. 3171 –3182, 2001. [Online]. Available: https://api.semanticscholar.org/CorpusID:7494.

[91] M. Bellazzini, F. F. Pecci, F. R. Ferraro, S. R. Galleti, M. Catelán, and W. B. Landsman, "Age as the second parameter in ngc 288/ngc 362? i. turnoff ages: A purely differential comparison," *The Astronomical Journal*, vol. 122, pp. 2569 –2586, 2001. [Online]. Available: https://api.semanticscholar.org/CorpusID:250807129.

[92] P. B. Stetson and W. E. Harris, "CCD Photometry of the Globular Cluster M92," AJ, vol. 96, p. 909, Sep. 1988. DOI: 10.1086/114856.

[93] G. Meylan, "Mass segregation in star clusters," *arXiv: Astrophysics*, 2000. [Online]. Available: https://api.semanticscholar.org/CorpusID:14207825.

[94] S. Monty, D. Yong, D. Massari, *et al.*, "Peeking beneath the precision floor – II. Probing the chemo-dynamical histories of the potential globular cluster siblings, NGC 288 and NGC 362," *Monthly Notices of the Royal Astronomical Society*, vol. 522, no. 3, pp. 4404–4420, Apr. 2023, ISSN: 0035-8711. DOI: 10.1093/mnras/stad1154. eprint: https://academic.oup.com/mnras/article-pdf/522/3/4404/56454048/stad1154.pdf. [Online]. Available: https://doi.org/10.1093/mnras/stad1154.

[95] Y. Momany, G. Piotto, A. Recio-Blanco, L. Bedin, S. Cassisi, and G. Bono, "A new feature along the extended blue horizontal branch of ngc 6752," *The Astrophysical Journal Letters*, vol. 576, p. L65, Dec. 2008. DOI: 10.1086/343125.

[96] R. Gratton, V. D'Orazi, A. Bragaglia, *et al.*, "The connection between missing agb stars and extended horizontal branches," *Astronomy and Astrophysics*, vol. 522, pp. 1–5, 2010. [Online]. Available: https://api.semanticscholar.org/CorpusID:119270903.

[97] S. Campbell, valentina d'orazi, T. Constantino, *et al.*, "The asymptotic giant branches of gcs: Selective entry only," *arXiv: Solar and Stellar Astrophysics*, pp. 101–104, 2013. [Online]. Available: https://api.semanticscholar.org/CorpusID:119220881.

[98] B. T. MacLean, S. W. Campbell, G. M. De Silva, *et al.*, "AGB subpopulations in the nearby globular cluster NGC 6397," *Monthly Notices of the Royal Astronomical Society*, vol. 475, no. 1, pp. 257–265, Dec. 2017, ISSN: 0035-8711. DOI: 10.1093/mnras/stx3217. eprint: https://academic.oup.com/mnras/article-pdf/475/1/257/23388378/stx3217.pdf. [Online]. Available: https://doi.org/10.1093/mnras/stx3217.

[99] S. Sahu, A. Subramaniam, P. Côté, N. K. Rao, and P. B. Stetson, "UVIT-HST-GAIA view of NGC 288: a census of the hot stellar population and its properties from UV," MNRAS, vol. 482, no. 1, pp. 1080–1095, Jan. 2019. DOI: 10.1093/mnras/sty2679. arXiv: 1810.01846 [astro-ph.SR].

[100] H. J. Farnhill, J. E. Drew, G. Barentsen, and E. A. González-Solares, "Calibrated and completeness-corrected optical stellar density maps of the northern Galactic plane," MNRAS, vol. 457, no. 1, pp. 642–665, Mar. 2016. DOI: 10.1093/mnras/stv2994. arXiv: 1601.02983 [astro-ph.GA].

[101] M. Bolte, "Mass Segregation in the Globular Cluster M30," ApJ, vol. 341, p. 168, Jun. 1989. DOI: 10.1086/167481.

[102] H. B. Richer, J. Anderson, J. Brewer, *et al.*, "Probing the Faintest Stars in a Globular Star Cluster," *Science*, vol. 313, no. 5789, pp. 936–940, Aug. 2006. DOI: 10.1126/science.1130691. arXiv: astro-ph/0702209 [astro-ph].